Noncanonical modulation of eIF2 pathway controls increase in local translation during neural wiring

Roberta Cagnetta[1], Hovy Ho-Wai Wong[1,6], Christian K. Frese[2,3,4], Giovanna R. Mallucci[5], Jeroen Krijgsveld[2,3], Christine E. Holt[1,7]*

[1]Department of Physiology Development and Neuroscience, Anatomy Building, University of Cambridge, Cambridge CB2 3DY, UK

[2]European Molecular Biology Laboratory (EMBL), 69117 Heidelberg, Germany

[3]German Cancer Research Center (DKFZ), 69121 Heidelberg, Germany

[4]CECAD Research Center, University of Cologne, 50931 Cologne, Germany

[5]UK Dementia Research Institute and Department of Clinical Neurosciences, Island Research Building, Cambridge Biomedical Campus, University of Cambridge, Cambridge CB2 0SL, UK

[6]Current address: Centre of Research in Neuroscience, The Research Institute of the McGill University Health Centre, Montreal General Hospital, Montréal, Québec H3A 2B4, Canada

[7]Lead Contact

*Correspondence: ceh33@cam.ac.uk (C.E.H.)

SUMMARY

Local translation is rapidly regulated by extrinsic signals during neural wiring but its control mechanisms remain elusive. Here, we show that the extracellular cue Sema3A induces an initial burst in local translation that precisely controls the phosphorylation of the translation initiation factor eIF2α via the Unfolded Protein Response (UPR) kinase, PERK. Strikingly, in contrast to canonical UPR signaling, the Sema3A-induced eIF2α phosphorylation bypasses global translational repression and underlies an increase in local translation through differential activity of eIF2B, mediated by Protein Phosphatase 1. Ultrasensitive proteomic analysis on axons reveals 75 proteins translationally controlled via the Sema3A-p-eIF2α pathway. These include proteostasis- and actin cytoskeleton-related proteins, but not canonical stress markers. Finally, we show that PERK signaling is needed for directional axon migration and visual pathway development *in vivo*. Thus, our findings reveal a noncanonical eIF2 signaling pathway that controls selective changes in axon translation and is required for neural wiring.

INTRODUCTION

Precise connectivity between neurons is needed to generate operative nervous systems. The initial assembly of neural circuits is mediated by the growth cone, a specialized structure at the tip of a growing axon, which senses extracellular cues along the pathway and transduces them into directional changes, thus navigating to its synaptic partner (Stoeckli, 2018; Jung et al., 2012). Once at the target, axons elaborate highly branched arbors and form synapses. The growth cone is often far from the soma and local mRNA translation mediates its rapid responses to extracellular cues (Campbell and Holt, 2001; Jung et al., 2012). Extrinsic cues, such as Semaphorin-3A (Sema3A), specifically remodel the nascent axonal proteome within just 5 min and orchestrate further dynamic changes over the next 25 min (Cagnetta et al., 2018). However, the translational mechanisms that control the cue-induced local nascent proteome remain elusive.

One way to control translation is to modulate one or more components of the translational

machinery. For instance, the α-subunit of the eukaryotic initiation factor 2 (eIF2α) mediates translational regulation in response to stress. eIF2α, GTP and the methionyl-initiator tRNA, constitute the ternary complex (eIF2·GTP·$tRNA_i^{Met}$), that is delivered to the ribosome. As GTP is hydrolyzed during each round of translation initiation, eIF2 recharges via the Guanine nucleotide Exchange Factor (GEF), eIF2B (Webb and Proud, 1997). Stress stimuli elicit phosphorylation of eIF2α at Ser51 via four possible kinases, including the PKR-like Endoplasmic Reticulum Kinase (PERK) (Holcik and Sonenberg, 2005). Upon phosphorylation, p-eIF2α binds to and inhibits its own GEF, eIF2B, whose concentration is much lower than eIF2. Therefore, eIF2B can no longer return p-eIF2 to its active GTP-bound state (Webb and Proud, 1997). This causes a reduction of the ternary complex available to reinitiate translation, which represses the translation of most mRNAs and selectively upregulates a small subset of mRNAs (~2.5% of total mRNAs; Dang do et al., 2009). This mechanism allows the cell to conserve resources and to translate transcripts involved in the cytoprotective response or, if the stress is prolonged, in apoptosis (Holcik and Sonenberg, 2005). For instance, Endoplasmic Reticulum (ER) stress phosphorylates eIF2α via PERK to turn on the Unfolded Protein Response (UPR), maintaining the homeostasis of the protein folding environment within the ER (Pavitt and Ron, 2012). Interestingly, Semaphorin signaling has been shown to govern epidermal morphogenesis via eIF2α dephosphorylation in *C. elegans* (Nukazuka et al. 2008), raising the possibility that Sema3A similarly employs the eIF2 pathway for local translation-dependent axon guidance in vertebrate neurons.

Here we investigate the role of eIF2α in regulating the nascent proteome in the axonal compartment of retinal ganglion cells (RGCs) in response to Sema3A. Our findings reveal a noncanonical PERK-p-eIF2α signaling pathway that underlies the Sema3A-induced *increase* in local protein synthesis and is required for neural wiring. Further, our results identify eIF2B modulation as a pivotal switch between the responses to stress and Sema3A.

RESULTS

Sema3A induces eIF2α phosphorylation in axons

The extracellular cue Sema3A induces protein synthesis-dependent chemotropic responses in axonal growth cones, peaking at 10 min post stimulation (Campbell and Holt, 2001; Campbell et al., 2001). Sema governs epidermal morphogenesis via eIF2α dephosphorylation *in C. elegans* (Nukazuka et al. 2008), prompting us to ask whether Sema3A similarly modulates eIF2α phosphorylation in axons. Quantitative immunofluorescence (qIF) revealed that Sema3A induces a significant increase in the p-eIF2α signal, but not in total-eIF2α, in retinal growth cones following 10 min stimulation (Figure 1A and 1B). The direction of the Sema-induced change in p-eIF2α was unexpectedly opposite to that seen in epidermal cells (Nukazuka et al. 2008) and was reminiscent of the p-eIF2α increase seen in the stress response. As a positive control, we compared the p-eIF2α signal in growth cones after stimulation with Sema3A *versus* treatment with the ER stress-inducing agent Thapsigargin (Tg), an inhibitor of the sarco/endoplasmic reticulum Ca^{2+} ATPase (Vuppalanchi et al., 2012). Consistent with data in fibroblasts (Sadighi Akha et al., 2011), a 15 min treatment with Tg induced an increase in p-eIF2α but not total-eIF2α in axons (Figure1A and 1B). Interestingly, in contrast to increased p-eIF2α levels that persist for hours in UPR signaling (Sadighi Akha et al., 2011), the increase with Sema3A treatment was rapid and transient, lasting minutes (Figure S1A). These data reveal that the physiological extracellular cue Sema3A triggers a rapid and transient phosphorylation of eIF2α in axons.

eIF2α phosphorylation differentially regulates translation in a stimulus-specific manner

Sema3A *increases* global translation locally in retinal axons (Campbell and Holt, 2001; Yoon et al., 2012). Yet, paradoxically, Sema3A stimulation results in increased p-eIF2α, which is known to *repress* global translation (Holcik and Sonenberg, 2005). Therefore, we next explored the role of p-eIF2α on Sema3A-induced global translation in growth cones. To this end, NSPs were tagged by puromycin pulse labeling (Schmidt et al., 2009). We stimulated with either Sema3A or the ER stressors Tg and Dithiothreitol (DTT), and co-treated with the pharmacological

reagent Integrated Stress Response Inhibitor (ISRIB). ISRIB stabilizes eIF2B, making eIF2B's GEF activity resistant to the effects of p-eIF2α without directly affecting eIF2α phosphorylation (Sidrauski et al., 2013; Sidrauski et al., 2015; Tsai et al., 2018). The released truncated puromycilated proteins were then quantified by IF using an anti-puromycin antibody. In accord with previous findings in whole cells (Sidrauski et al., 2013), Tg and DTT induced a decrease in the puromycin signal signifying a decrease in global translation in the growth cone, which was blocked by ISRIB, as expected (Figure 1C-D and S1B-C). Surprisingly, ISRIB completely abolished the Sema3A-induced *increase* in global translation, indicating that eIF2α phosphorylation also underlies the Sema3A-induced increase in protein synthesis in axons (Figure 1C-D). These results confirm that the stress response is conserved in axons (Vuppalanchi et al., 2012) and validate the mechanism of action of ISRIB in our system. Remarkably, they reveal that eIF2α phosphorylation can differentially regulate translation in a stimulus-specific manner.

Sema3A regulates a specific subset of axonal NSPs via eIF2α phosphorylation

We next investigated the proteins translationally regulated in the axon compartment of a single neuronal type (RGC) via the Sema3A-p-eIF2α pathway by employing pulsed Stable Isotope Labelling of Amino acids in Cell culture together with Single-Pot Solid-Phase-enhanced Sample Preparation (pSILAC-SP3; Hughes et al., 2014; Cagnetta et al., 2018). RGC axons grown on transwell filters were incubated for 1 h in depletion medium depleted of Lysine and Arginine, then severed from their cell bodies. Somaless axons were incubated for 15 min with Sema3A and 'heavy' isotope-coded amino acids (Lys8, Arg10) or with Sema3A, ISRIB and 'medium' isotope-coded amino acids (Lys4, Arg6) (Figure 2A). ISRIB makes eIF2B insensitive to p-eIF2α, thus focusing the window of sensitivity of pSILAC-SP3 on the axonal NSPs regulated by the Sema3A-p-eIF2α pathway. pSILAC-SP3 revealed 75 significant NSP changes mediated by Sema3A-p-eIF2α signaling (Figure 2B, Table S1). Intriguingly, Atf4 mRNA is resident in axons (Zivraj et al., 2010) and the upstream Open Reading Frames (uORFs) previously detected in mouse are conserved in its 5'UTR of *Xenopus laevis* and of mouse axons (Figure S2A-B). This

leads to the prediction that Atf4 is upregulated when eIF2α is phosphorylated and the level of ternary complex available to reinitiate translation decreases (Vattem and Wek, 2004). However, no upregulation of this classical stress marker was identified downstream of Sema3A-p-eIF2α signaling (Figure 2B, Table S1). This result was also confirmed by puromycilation of NSPs and Proximity Ligation Assay (puro-PLA; tom Dieck et al., 2015) in the presence of Sema3A, whereas Tg treatment increases the Atf4 puro-PLA signal (Figure S2C-D), suggesting that the Sema3A-p-eIF2α pathway generates a level of ternary complex higher than the canonical stress response.

KEGG pathway and functional Gene Ontology (GO) enrichment analyses revealed that the axonal NSPs regulated by Sema3A-p-eIF2α signaling encompass several functions (Figure 2C-D and S2E). eIF2α phosphorylation upregulates the KEGG pathway 'protein processing in ER', including Canx and Vcp, that are involved in protein folding and quality control (Figure 2C). NSPs belonging to 'metabolic pathways', including proteins for the biosynthesis of amino acids showed enhanced local translation (Figure 2C). Furthermore, eIF2α phosphorylation emerged to control the translation of some proteasomal subunits and ribosomal proteins (Figure 2C and S2E), possibly to remodel pre-existing proteasomes and ribosomes and confer substrate-specific functions (Shi et al., 2017; Padmanabhan et al., 2016). The Sema3A-p-eIF2α pathway also upregulates the 'barbed-end actin filament' GO term (Figure S2E), including the actin-binding protein Gelsolin, which has been previously shown to mediate filopodia retraction (Lu et al., 1997). The translational upregulation of Gelsolin and of the ribosomal protein RpL7a concur with their mRNA presence in embryonic axons (Table S1; Gumy et al., 2011) and were validated by qIF (Figure 2E-F). Network-based functional enrichment analysis revealed that some NSP changes constitute functionally coherent sets of mRNAs undergoing differential translation regulation (Figure 2D). Interestingly, two upregulated NSPs, Hspd1 and Vcp, belong to the 'response to misfolded proteins' GO term and 31 NSPs are members of the 'response to stress' GO term (Figure 2D). The Sema3A-p-eIF2α pathway also regulates several NSPs involved in the 'organization of the actin cytoskeleton', including β-actin (Figure 2D), whose

mRNA is present in retinal axons (Table S1; Zivraj et al., 2010) and whose downregulation was validated by qIF (Figure 2E-F). Collectively, comparison of the protein changes detected by pSILAC-SP3 *versus* the ones detected by qIF showed a strong positive correlation (r = 0.92, Figure 2G).

Next, we tested whether the NSPs controlled downstream of the Sema3A-p-eIF2α pathway are predicted to be regulated by other *trans*-acting translational regulators. We performed upstream regulator analysis based on previous datasets identifying targets of different translational regulators, including two canonical stress responses characterized in mouse liver downstream of the kinases PERK and GCN2. While only a very small fraction of targets was shared between Sema3A-p-eIF2α signaling and 4 out of 8 translational regulators (PERK, GCN2, mTOR, Apc), >85% of the NSPs was predicted to be specifically regulated by the Sema3A-p-eIF2α pathway (Figure S2F). Alternatively, differences between experimental systems (e.g. transcriptome specificity) might contribute to this limited overlap. These results identify the subset of axonal NSPs selectively regulated by the Sema3A-p-eIF2α pathway.

Sema3A-induced initial wave of local translation triggers eIF2α phosphorylation via PERK

Four kinases are known to phosphorylate eIF2α (PERK, PKR, HRI, GCN2) (Holcik and Sonenberg, 2005) prompting us to ask whether any of them is resident in retinal axons. PERK, PKR and HRI are annotated in *X. laevis* and IF indicated their presence in retinal axons (Figure 3A). Next, we asked which kinase is involved and how it is activated downstream of Sema3A. Within just 5 min, i.e. before eIF2α is phosphorylated (Figure S1A), Sema3A upregulates >60 significant axonal NSP changes, without apparent links to proteostasis (Cagnetta et al., 2018). By contrast, at 15 min, i.e. after eIF2α is phosphorylated (Figure S1A), the Sema3A-p-eIF2α pathway upregulates NSPs linked to the biosynthesis of amino acids (e.g. Pkm), ER and mitochondria protein quality control (e.g. the transitional ER ATPase Vcp), and chaperones (e.g. the ER chaperone Canx) (Figure 2B and 2C-D). This suggests a sequence of events in

which an initial p-eIF2α-independent wave of translation places a burden on the ER, which, in turn, activates the kinase PERK to trigger a counteracting translational control program to preserve the proteostasis. To test this hypothesis, first we blocked the Sema3A-induced burst in translation by the protein synthesis-inhibitor cycloheximide (CHX) and immunostained for total-eIF2α and p-eIF2α. Remarkably, CHX completely blocked the Sema3A-induced phosphorylation of eIF2α without affecting the level of total-eIF2α (Figure 3B-C), indicating that the up-regulation of local translation is required for eIF2α phosphorylation. In particular, we tested whether the mTOR- and ERK-1/2 (Extracellular signal-Regulated Kinase a.k.a. Mitogen-activated protein kinases p42/p44)-mediated initial wave of local translation, already active at 5 min Sema3A stimulation (Campbell and Holt, 2001; Campbell and Holt, 2003), underlies the phosphorylation of eIF2α. Co-treatment of axons with Sema3A and the mTOR inhibitor PP242 or the ERK-1/2 inhibitor U0126 completely inhibited the phosphorylation of eIF2α (Figure 3B-C), thus supporting the hypothesis. Each inhibitor on its own was sufficient to block eIF2α phosphorylation suggesting that there is a crosstalk between the ERK-1/2 and the mTOR pathways, in line with previous observations (Mendoza et al, 2011).

Finally, we stimulated axons with Sema3A in the presence of the PERK inhibitor GSK2606414 (GSK) and performed qIF for p-eIF2α. GSK blocked eIF2α phosphorylation (Figure 3D-E), revealing that PERK is activated by Sema3A. Consistent with our previous findings (Figure 1C-D), puromycilating the NSPs and co-treating with Sema3A and GSK phenocopied the effect of ISRIB by abolishing the Sema3A-induced increase in global translation (Figure 3F-G). To further verify these results, we knocked down PERK in embryos with a Morpholino (MO), which resulted in ~60% knock down (KD) (Figure S3), and we assayed global translation in response to Sema3A stimulation. The Sema3A-induced increase in global translation was completely inhibited in PERK morphants (Figure 3H-I). Thus, PERK can be activated in physiological conditions following an initial wave of local translation and is a crucial component of the Sema3A pathway to upregulate the local protein synthesis.

Local translation and dephosphorylation of eIF2Bε distinguish the Sema3A-induced response from the canonical stress response

Our findings revealed that the Sema3A response and the canonical UPR are both mediated by phosphorylation of eIF2α. Therefore, we investigated the mechanism underlying the differential translational control downstream of these two stimuli. p-eIF2α induced by Sema3A signaling, unlike canonical UPR, does not induce global translational repression (Figure 1C-D), nor the translation of classical stress markers such as Atf4 (Figure 2B and S2A-D), both of which are triggered by low levels of ternary complex. eIF2 recharges with GTP by eIF2B, which constitutes a rate-limiting factor for the ternary complex availability (Webb and Proud, 1997). Therefore, we hypothesized that, while inducing the phosphorylation of eIF2α, Sema3A may concomitantly modulate the GEF activity of eIF2B to alter the probability of generating the ternary complex. We reasoned that the modulation of eIF2B activity could be achieved in two non-mutually exclusive ways: (i) increasing the total amount of eIF2B available; (ii) adjusting the phosphorylation level of a conserved Ser residue on the subunit ε of eIF2B, wherein phosphorylation decreases eIF2B activity, whereas dephosphorylation increases eIF2B activity (Welsh et al., 1998; Quevedo et al., 2003). We first examined the level of total-eIF2Bε in the growth cone following Sema3A *versus* Tg treatment. qIF showed >35% increase in total-eIF2Bε in response to 10 min Sema3A, but not Tg (Figure 4A-B). This rapid increase could result from local translation since eIF2Bε mRNA resides in retinal axons (Figure 4C). CHX blocked the Sema3A-induced increase in eIF2Bε (Figure 4A-B) indicating that eIF2Bε, unlike eIF2α (Figure 3A-B), is locally translated in response to Sema3A. This finding is in accord with the detection of eIF2Bε mRNA translation in mouse retinal axons in the tectum *in vivo*, where Sema3A controls neural connectivity (Shigeoka et al., 2016). Like reticulocytes where the eIF2:eIF2B ratio is 7:1 (Webb and Proud, 1997), eIF2B ε is much less abundant than eIF2α in axons as indicated by the inability of the pSILAC-SP3 approach to detect either nascent or pre-existing eIF2B ε protein whereas eIF2α protein is readily detected (Cagnetta et al., 2018). Since Sema3A is known to activate axonal mTOR and ERK-1/2 within 5 min stimulation (Campbell

and Holt, 2001; Campbell and Holt, 2003), we asked whether these translational regulators control eIF2Bε rapid local translation. The results showed that eIF2Bε increases within just 5 min of Sema3A stimulation, but this is not mediated by mTOR nor ERK-1/2 (Figure S4A-B). The negative control showed that co-treatment with ISRIB does not affect eIF2Bε increase (Figure S4A-B), consistent with the lack of eIF2α phosphorylation at 5 min stimulation (Figure S1A). Upstream regulator analysis based on previous datasets identifying the targets of several translational regulators predicted that neither Apc, Mena, Fmrp, Tdp43, Fus nor mTOR control eIF2Bε translation.

We next examined the level of phosphorylation of eIF2Bε, which regulates eIF2B activity. We stimulated with Sema3A for 10 min and immunostained growth cones for p-eIF2Bε (Ser539). qIF showed ~35% decrease in p-eIF2Bε in response to Sema3A but not Tg (Figure 4D-E). Previous work has shown in rat cortical neurons that dephosphorylation of p-eIF2Bε can be mediated by Protein Phosphatase 1 (PP1) activation following its interaction with ERK-1/2 (Quevedo et al., 2003), which constitutes a major component of the Sema3A intracellular pathway (Campbell and Holt, 2003). Therefore, we tested whether PP1 is responsible for eIF2Bε dephosphorylation by co-treating with Sema3A and Tautomycin (TM), which preferentially inhibits PP1 (MacKintosh and MacKintosh, 1994). TM abolished the Sema3A-induced dephosphorylation of eIF2Bε (Figure 4D-E), thus revealing that Sema3A activates PP1 to mediate eIF2Bε dephosphorylation. By contrast, PP1 does not regulate eIF2α phosphorylation level (Figure S4C-D), indicating a lack of involvement of the PP1-eIF2α-recruiting scaffold protein GADD34 (Growth Arrest and DNA Damage-inducible protein) at 10 min Sema3A stimulation (Choy et al., 2015). Finally, we tested whether ERK-1/2 is upstream of eIF2Bε dephosphorylation by co-treating with Sema3A and U0126, and immunostaining for p-eIF2Bε. Interestingly, the results revealed that the dephosphorylation of eIF2Bε switches to phosphorylation (Figure 4D-E). This, together with previous studies in cortical neurons, suggests that ERK-1/2 activates PP1 and simultaneously suppresses the activity of GSK-3β (Quevedo et al., 2003; Hetman et al., 2002), which is known to phosphorylate eIF2Bε and to be

repressed at low Sema3A concentrations in a dose-dependent manner (Welsh et al., 1998; Manns et al., 2012).

To further test whether eIF2B activity represents a key node between the UPR and Sema3A differential translation control, we asked whether it is possible to switch the Sema3A-induced global translation upregulation to repression by only modulating eIF2B activity. To this end we puromycilated the NSPs and stimulated with Sema3A in the presence of TM, which inhibits eIF2Bε dephosphorylation (Figure 4D-E) and thereby blocks its increase in activity. Strikingly, the Sema3A-induced rapid increase in global translation switched to repression (Figure 4F-G), thus mimicking the effects of the Tg- and DTT-induced stress response (Figure 1C-D, Figure S1B-C). This result indicates that the Sema3A-induced local increase in total-eIF2Bε (Figure 4A-B) on its own is not sufficient to increase the eIF2B overall GEF activity and that the Sema3A-induced phosphorylation of eIF2α underlies the increase in global translation by engaging the eIF2Bε dephosphorylation. Finally, we asked whether this translational control mechanism is detectable also in the developing nervous system *in vivo*. We incubated brains of embryos at a stage when Sema3A is known to act on retinal axons (stage 35/36; Campbell et al., 2001) with TM for 30 min, puromycilated NSPs over the last 15 min of the treatment and carried out western blot to probe for puromycin. The results showed a decrease in the global translation equal to ~25% (Figure 4H-I), indicating that translation mediated by p-eIF2α-eIF2Bε signaling occurs in the developing brain *in vivo*. Altogether, the findings indicate that during neurodevelopment Sema3A-induced phosphorylation of axonal eIF2α underlies the noncanonical increase in global translation by enhancing eIF2B activity primarily through dephosphorylation of its ε subunit.

Sema3A-induced polarized phosphorylation of eIF2α is required for directional migration

We next explored the functional significance of eIF2α phosphorylation downstream of Sema3A. pSILAC-SP3 had revealed that Sema3A-p-eIF2α signaling controls the translation of several

proteins involved in the regulation of the actin cytoskeleton and in axon guidance (Figure 2D). For example, the Sema3A-p-eIF2α pathway upregulates Gelsolin (Figure 2B and 2E-F), an actin-binding protein required for filopodia retraction (Lu et al., 1997) and L1cam, a cell adhesion molecule necessary for topographic mapping of retinal axons (Demyanenko and Maness, 2003). Therefore, we investigated whether phosphorylation of eIF2α plays a role in the Sema3A-induced chemorepulsion. We carried out growth cone turning assays with a polarized gradient of Sema3A and bath-applied ISRIB or GSK. Both treatments blocked the Sema3A-induced repulsive turning (Figure 5A-B and S5A). In somaless axons, the repulsive turning was also inhibited by ISRIB (Figure 5C-D and S5B), indicating that the local phosphorylation of eIF2α mediates the Sema3A-induced chemorepulsion. Since the Sema3A-p-eIF2α-mediated increase in translation is dictated by eIF2Bε dephosphorylation (Figure 4D-G), we tested whether blocking PP1 also affects the Sema3A-induced repulsive turning. Bath-application of TM inhibited the chemorepulsion (Figure 5A-B and S5A).

In light of these results, we reasoned that during the chemotropic response a directional stimulus of Sema3A might produce a polarized asymmetrical phosphorylation of eIF2α, thus generating an internal gradient of proteomic change across the growth cone. To test this possibility, a gradient of Sema3A was applied for 10 min at a 90° angle to the growth cone as an assay to achieve a steep difference between the 'near' and the 'far' sides of the growth cone (Figure 5E). qIF indicated that a Sema3A gradient significantly increases eIF2α phosphorylation on the near-stimulus side (Figure 5E-F and S5C). Further confirmation of the asymmetrical phosphorylation was obtained by comparing the center-of-mass value of p-eIF2α IF signal between the control and Sema3A gradient conditions, which revealed an equivalent shift towards the Sema3A source (Figure 5G and S5D). These results, together with the finding that Sema3A downregulates β-actin via p-eIF2α (Figure 2B and 2E-F), are consistent with previous work showing that β-actin decreases on the near-stimulus side in response to a polarized gradient of Sema3A (Cagnetta et al., 2018) and support a growth cone repulsive model where p-eIF2α increases on the side close to the source of Sema3A to mediate

cytoskeleton disassembly and filopodia collapse (Figure 5H). Collectively, the data show that polarized phosphorylation of eIF2α within the growth cone is required for the Sema3A-induced directional migration.

PERK signaling is involved in retinotectal axon navigation *in vivo*

We next investigated whether eIF2α phosphorylation is involved in the navigation of retinal axons *in vivo*. The PERK MO was injected into only one of the two dorsal blastomeres, leading to embryos in which one half of the central nervous system (CNS) is depleted of PERK and the other half is wild type (Figure 6A) (Roque et al., 2016). During development, RGC axons cross the midline at the optic chiasm and project contralaterally, therefore DiI injection in the ipsilateral eye enabled to test the contribution of axonal PERK in RGCs only, without affecting the optic tract substrate (Figure 6A-B). Embryos injected with PERK MO overall appeared to develop normal projections as in the Control MO (CoMO) (Figure 6C-D), showing no difference in the optic tract width (Figure S6A-B). PERK morphants exhibited a slight decrease (not statistically significant) in the mid-diencephalic turn (MDT) angle (Figure 6B, 6H and S6C) and an increase in the proportion of embryos with a MDT angle smaller than in the wild-type (i.e. MDT < 45°) (Figure 6I). Measurement of the tectal projection angle (TPA) (Figure 6B) revealed an increased tendency of axons to turn away from the posterior tectal border (not statistically significant; Figure 6J-K and S6D). Collectively, this result was in line with previous studies showing in the same *Xenopus* visual system that no gross abnormalities were observed in axon navigation after either Sema3A KD or acute inhibition of protein synthesis (Atkinson-Leadbeater et al., 2010; Wong et al., 2017). Similarly, the retinotectal projection did not exhibit evident defects after genetic deletion or pharmacological inhibition of mTOR in zebrafish (Cioni et al., 2018).

Previous work has shown that Sema3A and Slit1 transcripts are both present at the mid-diencephalic turn and in the tectum, and that these two cues cooperate to guide the turning of axons caudally (Campbell et al., 2001; Hocking et al., 2010; Atkinson-Leadbeater et al., 2010).

Furthermore, a recent study in mouse dorsal root ganglion growth cones has found that Sema3A and Slit1 induce chemorepulsion through distinct mechanisms (McConnell et al., 2016). Therefore, we reasoned that Slit1 might act via a PERK-independent route and compensate PERK KD downstream of Sema3A. We first tested whether Slit1 affects eIF2α phosphorylation. Interestingly, qIF showed no change in the growth cone basal p-eIF2α level after Slit1 stimulation (Figure S6E-F), thus indicating that PERK is selectively activated downstream of Sema3A. Next, we tested Slit1 MO in our system (~55% KD) (Figure S6G) and knocked down Slit1 in the optic tract substrate *in vivo* (Figure 6A). Consistent with previous results (Atkinson-Leadbeater et al., 2010), Slit1 KD did not interfere with the optic tract width (Figure 6C, 6E and S5B) or with navigation (Figure 6C, 6E, 6H-K, S6C-D). We then knocked down, simultaneously, PERK in the axon and Slit1 in the optic tract substrate (Figure 6A). Remarkably, DiI axon labeling revealed that, although the optic tract width remained unaffected (Figure S6B), the whole axonal bundle failed to turn caudally (Figure 6F-I and S6C) and did not correctly enter the tectum in the midbrain (Figure 6F-G, 6J-K and S6D).

Further, we exposed the intact brain to ISRIB treatment by removal of the overlying epidermis during the period of optic pathway formation (Figure S6H). In line with the PERK morphants, the results showed no significant difference in the optic tract width, MDT angle and tectal entry (Figure S6I-J, S6L-M). When ISRIB treatment was combined with Slit1 KD in the optic tract substrate (Figure S6H), the brains exhibited axon guidance defects that phenocopied those seen with PERK-Slit KD (Figure S6K, S6M-N), without affecting the optic tract width (Figure S6L). Collectively, the data indicate that PERK-p-eIF2α signaling cooperates with other p-eIF2α-independent pathways in guidance cue integration during retinotectal axon navigation *in vivo*.

PERK signaling is required for axonal branching *in vivo*

On reaching the tectum, where Sema3A is expressed (Campbell et al., 2001), RGC axons elaborate terminal branches and form synapses. Sema3A has been shown to elicit branching

of retinal and GABAergic axons (Campbell et al., 2001; Cioni et al., 2013) and axon branching is dependent on local protein synthesis *in vivo* (Wong et al., 2017), leading us to ask whether eIF2α phosphorylation is required for branching *in vivo*. The PERK MO and a mGFP reporter were co-electroporated into the eye at stage 28 and single axon arbors were imaged at stage 45 (Wong et al., 2017). While CoMO-electroporated axons exhibited complex arbors, PERK MO axons exhibited much simpler arbor architecture (Figure 6L). Quantitative analysis revealed that the branch numbers decreased across different branch orders, leading to an overall drop of 56% (Figure 6M). Furthermore, a 55% reduction of the total branch length was observed (Figure 6N). The Axon Complexity Index (ACI) (Figure 6O; Marshak et al., 2007) showed a marked decrease in the PERK morphants (Figure 6P). These data reveal that PERK signaling is required for developing axon arbor complexity *in vivo*.

DISCUSSION

Extracellular stimuli can rapidly remodel the local nascent proteome in axons and here we investigated the underlying translational control mechanisms and mRNA targets. We used nascent proteome analysis combined with *in vitro* and *in vivo* models to demonstrate that a Sema3A-induced initial wave of local translation triggers a noncanonical eIF2 signaling pathway, which upregulates local translation and orchestrates a set of proteomic changes required for axon guidance and neural connectivity.

A canonical role for eIF2α phosphorylation in physiological conditions, rather than in response to stress or in pathology, has already emerged from recent studies (Di Prisco et al., 2014; Dalton et al., 2013; Trinh et al., 2014; Woo et al., 2012). Our work differs in showing for the first time that eIF2α phosphorylation can underlie an *increase* in translation, as opposed to the decrease characterizing the canonical stress model. Notably, our results show that eIF2α phosphorylation (10 min) is dependent on the Sema3A-induced initial wave (≥ 5 min) of protein synthesis mediated by mTOR and ERK-1/2 (Figure 7). These findings support a model where the ER, known to reside throughout the axon (Wu et al., 2017), becomes overloaded with new

unfolded (i.e. yet-to-be folded) proteins following Sema3A stimulation (~30% increase in global translation within only 10 min). This may cause a physiological stress, which activates the ER stress sensor, PERK, and leads to eIF2α phosphorylation. This model is further supported by the downstream selective translation of NSPs involved in protein folding, ER and mitochondria protein quality control, and biosynthesis of amino acids, possibly to sustain the burst in global translation. Interestingly, ERK-1/2 also controls eIF2Bε, likely by activating PP1 and suppressing GSK-3β (Figure 7) (Quevedo et al., 2003; Hetman et al., 2002). Therefore, the findings reveal a dependency between the pathways triggered downstream of Sema3A, wherein p-eIF2α-eIF2Bε signaling can be activated at the second stage of a cascade, and account for the dynamic and changing nature of the nascent axonal proteome during the 30 min post-stimulation (Cagnetta et al., 2018).

The phosphorylation status of eIF2Bε, and hence the GEF activity of eIF2B (Quevedo et al., 2003), dictates the outcome of the global translation levels distinguishing the response to Sema3A from the canonical UPR. Specifically, we found that Sema3A, unlike Tg, induces the local translation and dephosphorylation of eIF2Bε via PP1 (Figure 7). The absence of Atf4 upregulation suggests that the Sema3A-induced regulation of eIF2B and eIF2α phosphorylation precisely influences the rate of generation of the ternary complex, promoting higher exchange of GDP for GTP on eIF2 than in the canonical stress response, which is instead triggered by low levels of ternary complex (Vattem and Wek, 2004). One possibility is that increased eIF2B activity exchanges GDP for GTP with higher efficiency than in the canonical UPR on the subpopulation of eIF2 that escapes phosphorylation on its α-subunit. A further possibility is that dephosphorylation of eIF2Bε may stabilize the eIF2B dimer decreasing its affinity for p-eIF2α and permitting higher GDP-GTP exchange than in the canonical UPR, similar to the mechanism of action of ISRIB (Tsai et al., 2018; Sidrauski et al., 2015). This bypasses the global translational repression and the uORFs-mediated upregulation of canonical ER stress markers, and regulates the translational efficiency of a subset of mRNAs possibly sensitive to such levels of ternary complex (Figure 7). It is interesting to speculate that this translational

control mechanism may be employed also by other biological processes to tackle large increases in protein synthesis (Baleriola et al., 2014) and consequent ER overload, bypassing the translation of pro-apoptotic factors (e.g. Chop; Woo et al., 2012) and regulating the translation of a specific subset of mRNAs (e.g. for the proteostasis). Furthermore, this noncanonical way to control translation may suggest new therapeutic targets for disorders involving the detrimental expression of UPR markers and pathogenic translation repression (Moreno et al., 2012; Ma et al., 2013).

Our study also revealed that a physiological extracellular stimulus can control the phosphorylation of eIF2α in axons with spatio-temporal precision. The phosphorylation is polarized to the near-stimulus compartment of the growth cone, indicating that its translational control mechanism can be further spatially compartmentalized at the subcellular level (Figure 5H). Of particular interest, the Sema3A-induced phosphorylation of eIF2α is transient, peaking at 10 min post-stimulation and declining thereafter, which is in contrast to the canonical stress response where eIF2α phosphorylation typically peaks at 30 min and endures for hours (Sadighi Akha et al., 2011). The phosphatase PP2Cα topped the list of selectively upregulated nascent proteins in response to Sema3A via p-eIF2α. PP2Cα dephosphorylates and thereby inhibits the 5' adenosine monophosphate-activated protein kinase (AMPK) (Lammers and Lavi, 2007), which has been reported to be required for PERK activation in a specific UPR pathway but not in response to Tg (Yang et al., 2013). This raises the possibility that Sema3A turns off the PERK-p-eIF2α pathway with an in-built negative feedback loop by triggering the local translation of PP2Cα, thus accounting for the eIF2α transient phosphorylation. This fast mechanism could accommodate the rapid cue-induced response locally, likely required *in vivo* for the growing axons to make timely navigational and connectivity decisions.

PERK signaling is involved in the axon retinotectal navigation *in vivo* by working at the mid-diencephalic turn and in the tectum together with Slit1, whose downstream signaling pathway is p-eIF2α-independent. This mechanism may have evolved to build a more robust system and

increase the axon navigation accuracy. PERK signaling is also required for axon arbor formation in the tectum, in line with recent *in vivo* evidence showing that acute inhibition of protein synthesis impairs axonal branching (Wong et al., 2017). Importantly, given that the axons are exposed to various guidance cues in the tectum, we do not exclude the interesting possibility that PERK may act downstream of further extracellular stimuli that, like Sema3A, induce a strong global increase in local translation (Yoon et al., 2012).

Lastly, some of the NSPs regulated via Sema3A-p-eIF2α signaling are neurological disease-associated (Table S2), suggesting links between defective axonal translational control in neural wiring and disease. In addition, Sema3A is known to inhibit axon regeneration following injury in the adult nervous system (Giger et al., 2010), hence the eIF2 pathway may represent a therapeutic target for neural repair. In conclusion, the noncanonical signaling reported could open new avenues of investigation in translational control and lead to a better understanding of neural wiring and potentially help developing new therapeutic approaches.

ACKNOWLEDGMENTS

We thank D. Ron, S.J. Marciniak and J.E. Chambers for their initial input and sharing reagents, M. Halliday, C.G. Roque and W.A. Harris for valuable discussions, T. Shigeoka for the heat map diagram, K. Mooslehner, A. Dwivedy, A. Bellon and J.Q. Lin for technical assistance. This work was supported by Wellcome Trust Grants (085314/Z/08/Z; RG84912) and ERC Advanced Grant (322817) (C.E.H.), BBSRC (RG68461) (R.C.), EMBO postdoctoral fellowship (LTF1006-2013) (C.K.F.), Excellence Cluster CellNetworks (J.K.), ERC Consolidator Award UPR Neuro and UK DRI Award (G.R.M.), Cambridge Trust, Croucher Foundation, Sir Edward Youde Memorial Fund (H.H.W.).

AUTHOR CONTRIBUTIONS

R.C. and C.E.H. conceived the project and wrote the manuscript. R.C. designed the

experimental strategy. R.C. performed puromycilation assay, qIF, RT-PCR, pSILAC, bioinformatic analyses, puro-PLA, growth cone gradient assay, western blot, blastomere injection and DiI. H.H.W. performed electroporation and branching experiment. C.K.F. carried out SP3-MS and proteomics data processing. All the authors commented on the manuscript. C.E.H., J.K. and G.R.M. supervised the project.

DECLARATION OF INTERESTS

The authors declare no competing interests.

REFERENCES

Atkinson-Leadbeater, K., Bertolesi, G. E., Hehr, C. L., Webber, C. A., Cechmanek, P. B. & McFarlane, S. (2010) Dynamic expression of axon guidance cues required for optic tract development is controlled by fibroblast growth factor signaling. J Neurosci, 30(2), 685-93.

Baleriola, J., Walker, C. A., Jean, Y. Y., Crary, J. F., Troy, C. M., Nagy, P. L. & Hengst, U. (2014) Axonally synthesized ATF4 transmits a neurodegenerative signal across brain regions. Cell, 158(5), 1159-1172.

Cagnetta, R., Frese, C. K., Shigeoka, T., Krijgsveld, J. & Holt, C. E. (2018) Rapid cue-specific remodeling of the nascent axonal proteome. Neuron, 99(1), 29-46.e4.

Campbell, D. S. and Holt, C. E. (2001) Chemotropic responses of retinal growth cones mediated by rapid local protein synthesis and degradation, Neuron, 32(6), 1013-26.

Campbell, D. S. & Holt, C. E. (2003) Apoptotic pathway and MAPKs differentially regulate chemotropic responses of retinal growth cones. Neuron, 37(6), 939-52.

Campbell, D. S., Regan, A. G., Lopez, J. S., Tannahill, D., Harris, W. A. & Holt, C. E. (2001) Semaphorin 3A elicits stage-dependent collapse, turning, and branching in Xenopus retinal growth cones. J Neurosci, 21(21), 8538-47.

Choy, M. S., Yusoff, P., Lee, I. C., Newton, J. C., Goh, C. W., Page, R., Shenolikar, S. & Peti, W. (2015) Structural and Functional Analysis of the GADD34:PP1 eIF2α Phosphatase. Cell Rep, 11(12), 1885-91.

Cioni, J. M., Telley, L., Saywell, V., Cadilhac, C., Jourdan, C., Huber, A. B., Huang, J. Z., Jahannault-Talignani, C. & Ango, F. (2013) SEMA3A signaling controls layer-specific interneuron branching in the cerebellum. Curr Biol, 23(10), 850-61.

Cioni, J. M., Wong, H. H., Bressan, D., Kodama, L., Harris, W. A. & Holt, C. E. (2018) Axon-axon interactions regulate topographic optic tract sorting via CYFIP2-dependent WAVE complex function. Neuron, 97(5), 1078-1093.e6.

Colombrita, C., Onesto, E., Megiorni, F., Pizzuti, A., Baralle, F. E., Buratti, E., Silani, V. & Ratti, A. (2012) TDP-43 and FUS RNA-binding proteins bind distinct sets of cytoplasmic messenger RNAs and differently regulate their post-transcriptional fate in motoneuron-like cells. J Biol Chem, 287(19), 15635-47.

Cox, J. and Mann, M. (2008) MaxQuant enables high peptide identification rates, individualized p.p.b.-range mass accuracies and proteome-wide protein quantification. Nat. Biotechnol. 26,1367–72.

Dalton, R. P., Lyons, D. B. & Lomvardas, S. (2013) Co-opting the unfolded protein response to elicit olfactory receptor feedback. Cell, 155(2), 321-32.

Dang Do, A. N., Kimball, S. R., Cavener, D. R. & Jefferson, L. S. (2009) eIF2alpha kinases GCN2 and PERK modulate transcription and translation of distinct sets of mRNAs in mouse liver. Physiol Genomics, 38(3), 328-41.

Darnell, J. C., Van Driesche, S. J., Zhang, C., Hung, K. Y., Mele, A., Fraser, C. E., Stone, E. F., Chen, C., Fak, J. J., Chi, S. W. et al. (2011) FMRP stalls ribosomal translocation on mRNAs linked to synaptic function and autism. Cell, 146(2), 247-61.
Di Prisco, G. V., Huang, W., Buffington, S. A., Hsu, C. C., Bonnen, P. E., Placzek, A. N., Sidrauski, C., Krnjević, K., Kaufman, R. J., Walter, P., et al. (2014) Translational control of mGluR-dependent long-term depression and object-place learning by eIF2α. Nat Neurosci, 17(8), 1073-82.
Giger, R. J., Hollis, E. R. & Tuszynski, M. H. (2010) Guidance molecules in axon regeneration. Cold Spring Harb Perspect Biol, 2(7), 1-21.
Gumy, L. F., Yeo, G. S., Tung, Y. C., Zivraj, K. H., Willis, D., Coppola, G., Lam, B. Y., Twiss, J. L., Holt, C. E. and Fawcett, J. W. (2011) Transcriptome analysis of embryonic and adult sensory axons reveals changes in mRNA repertoire localization, RNA, 17(1), 85-98.
Hetman, M., Hsuan, S. L., Habas, A., Higgins, M. J. & Xia, Z. (2002) ERK1/2 antagonizes glycogen synthase kinase-3beta-induced apoptosis in cortical neurons. J Biol Chem, 277(51), 49577-84.
Hocking, J. C., Hehr, C. L., Bertolesi, G. E., Wu, J. Y. & McFarlane, S. (2010) Distinct roles for Robo2 in the regulation of axon and dendrite growth by retinal ganglion cells. Mech Dev, 127(1-2), 36-48.
Holcik, M. & Sonenberg, N. (2005) Translational control in stress and apoptosis. Nat Rev Mol Cell Biol, 6(4), 318-27.
Hughes, C. S., Foehr, S., Garfield, D. A., Furlong, E. E., Steinmetz, L. M. and Krijgsveld, J. (2014) Ultrasensitive proteome analysis using paramagnetic bead technology, Mol Syst Biol, 10, 757.
Jung, H., Yoon, B. C. & Holt, C. E. (2012) Axonal mRNA localization and local protein synthesis in nervous system assembly, maintenance and repair. Nat Rev Neurosci, 13(5), 308-24.
Lammers, T. & Lavi, S. (2007) Role of type 2C protein phosphatases in growth regulation and in cellular stress signaling. Crit Rev Biochem Mol Biol, 42(6), 437-61.
Lohof, A. M., Quillan, M., Dan, Y. & Poo, M. M. (1992) Asymmetric modulation of cytosolic cAMP activity induces growth cone turning. J Neurosci, 12(4), 1253-61.
Lu, M., Witke, W., Kwiatkowski, D. J. & Kosik, K. S. (1997) Delayed retraction of filopodia in gelsolin null mice. J Cell Biol, 138(6), 1279-87.
Ma, T., Trinh, M. A., Wexler, A. J., Bourbon, C., Gatti, E., Pierre, P., Cavener, D. R. & Klann, E. (2013) Suppression of eIF2α kinases alleviates Alzheimer's disease-related plasticity and memory deficits. Nat Neurosci, 16(9), 1299-305.
MacKintosh, C. and MacKintosh, R. W. (1994) Inhibitors of protein kinases and phosphatases, Trends Biochem Sci, 19(11), 444-8.
Manns, R. P., Cook, G. M., Holt, C. E. & Keynes, R. J. (2012) Differing semaphorin 3A concentrations trigger distinct signaling mechanisms in growth cone collapse. J Neurosci, 32(25), 8554-9.
Marshak, S., Nikolakopoulou, A.M., Dirks, R., Martens, G.J., and Cohen-Cory, S. (2007). Cell-autonomous TrkB signaling in presynaptic retinal ganglion cells mediates axon arbor growth and synapse maturation during the establishment of retinotectal synaptic connectivity. J. Neurosci. 27, 2444-2456.
McConnell, R. E., Edward van Veen, J., Vidaki, M., Kwiatkowski, A. V., Meyer, A. S. & Gertler, F. B. (2016) A requirement for filopodia extension toward Slit during Robo-mediated axon repulsion. J Cell Biol, 213(2), 261-74.
Mendoza, M. C., Er, E. E. & Blenis, J. (2011) The Ras-ERK and PI3K-mTOR pathways: cross-talk and compensation. Trends Biochem Sci, 36(6), 320-8.
Moreno, J. A., Radford, H., Peretti, D., Steinert, J. R., Verity, N., Martin, M. G., Halliday, M., Morgan, J., Dinsdale, D., Ortori, C. A., et al. (2012) Sustained translational repression by eIF2α-P mediates prion neurodegeneration. Nature, 485(7399), 507-11.
Nieuwkoop, P.D., and Faber, J. (1994). Normal table of Xenopus laevis (Daudin): A Systematical and Chronological Survey of the Development from the Fertilized Egg till the End of Metamorphosis (Garland).

Nukazuka, A., Fujisawa, H., Inada, T., Oda, Y. & Takagi, S. (2008) Semaphorin controls epidermal morphogenesis by stimulating mRNA translation via eIF2alpha in Caenorhabditis elegans. Genes Dev, 22(8), 1025-36.
Padmanabhan, A., Vuong, S. A. and Hochstrasser, M. (2016) Assembly of an Evolutionarily Conserved Alternative Proteasome Isoform in Human Cells, Cell Rep, 14(12), 2962-74.
Pavitt, G. D. & Ron, D. (2012) New insights into translational regulation in the endoplasmic reticulum unfolded protein response. Cold Spring Harb Perspect Biol, 4(6).
Preitner, N., Quan, J., Nowakowski, D. W., Hancock, M. L., Shi, J., Tcherkezian, J., Young-Pearse, T. L. & Flanagan, J. G. (2014) APC is an RNA-binding protein, and its interactome provides a link to neural development and microtubule assembly. Cell, 158(2), 368-82.
Quevedo, C., Salinas, M. & Alcázar, A. (2003) Initiation factor 2B activity is regulated by protein phosphatase 1, which is activated by the mitogen-activated protein kinase-dependent pathway in insulin-like growth factor 1-stimulated neuronal cells. J Biol Chem, 278(19), 16579-86.
Ritchie, M.E., Phipson, B., Wu, D., Hu, Y., Law, C.W., Shi, W., Smyth, G.K. (2015) limma powers differential expression analyses for RNA-sequencing and microarray studies. Nucleic Acids Res. 43, e47.
Roque, C. G., Wong, H. H., Lin, J. Q. & Holt, C. E. (2016) Tumor protein Tctp regulates axon development in the embryonic visual system. Development, 143(7), 1134-48.
Sadighi Akha, A. A., Harper, J. M., Salmon, A. B., Schroeder, B. A., Tyra, H. M., Rutkowski, D. T. & Miller, R. A. (2011) Heightened induction of proapoptotic signals in response to endoplasmic reticulum stress in primary fibroblasts from a mouse model of longevity. J Biol Chem, 286(35), 30344-51.
Schmidt, E. K., Clavarino, G., Ceppi, M. & Pierre, P. (2009) SUnSET, a nonradioactive method to monitor protein synthesis. Nat Methods, 6(4), 275-7.
Shigeoka, T., Jung, H., Jung, J., Turner-Bridger, B., Ohk, J., Lin, J. Q., Amieux, P. S. and Holt, C. E. (2016) Dynamic Axonal Translation in Developing and Mature Visual Circuits, Cell, 166(1), 181-92.
Shi, Z., Fujii, K., Kovary, K. M., Genuth, N. R., Rˆst, H. L., Teruel, M. N. & Barna, M. (2017) Heterogeneous Ribosomes Preferentially Translate Distinct Subpools of mRNAs Genome-wide. Mol Cell.
Sidrauski, C., Acosta-Alvear, D., Khoutorsky, A., Vedantham, P., Hearn, B. R., Li, H., Gamache, K., Gallagher, C. M., Ang, K. K., Wilson, C., et al. (2013) Pharmacological brake-release of mRNA translation enhances cognitive memory. Elife, 2, e00498.
Sidrauski, C., Tsai, J. C., Kampmann, M., Hearn, B. R., Vedantham, P., Jaishankar, P., Sokabe, M., Mendez, A. S., Newton, B. W., Tang, E. L., et al. (2015) Pharmacological dimerization and activation of the exchange factor eIF2B antagonizes the integrated stress response. Elife, 4, e07314.
Stoeckli, E. T. (2018) Understanding axon guidance: are we nearly there yet? Development, 145(10).
Thoreen, C. C., Chantranupong, L., Keys, H. R., Wang, T., Gray, N. S. & Sabatini, D. M. (2012) A unifying model for mTORC1-mediated regulation of mRNA translation. Nature, 485(7396), 109-13.
Trinh, M. A., Ma, T., Kaphzan, H., Bhattacharya, A., Antion, M. D., Cavener, D. R., Hoeffer, C. A. & Klann, E. (2014) The eIF2α kinase PERK limits the expression of hippocampal metabotropic glutamate receptor-dependent long-term depression. Learn Mem, 21(5), 298-304.
tom Dieck, S., Kochen, L., Hanus, C., Heum¸ller, M., Bartnik, I., Nassim-Assir, B., Merk, K., Mosler, T., Garg, S., Bunse, S., et al. (2015) Direct visualization of newly synthesized target proteins in situ, Nat Methods, 12(5), 411-4.
Tsai, J. C., Miller-Vedam, L. E., Anand, A. A., Jaishankar, P., Nguyen, H. C., Renslo, A. R., Frost, A. & Walter, P. (2018) Structure of the nucleotide exchange factor eIF2B reveals mechanism of memory-enhancing molecule. Science, 359(6383).
Turner-Bridger, B., Jakobs, M., Muresan, L., Wong, H. H., Franze, K., Harris, W. A. & Holt, C. E. (2018) Single-molecule analysis of endogenous β-actin mRNA trafficking reveals a

mechanism for compartmentalized mRNA localization in axons. Proc Natl Acad Sci U S A, 115(41), E9697-E9706.
Vattem, K. M. & Wek, R. C. (2004) Reinitiation involving upstream ORFs regulates ATF4 mRNA translation in mammalian cells. Proc Natl Acad Sci U S A, 101(31), 11269-74.
Vidaki, M., Drees, F., Saxena, T., Lanslots, E., Taliaferro, M. J., Tatarakis, A., Burge, C. B., Wang, E. T. & Gertler, F. B. (2017) A requirement for Mena, an actin regulator, in local mRNA translation in developing neurons. Neuron, 95(3), 608-622.e5.
Vizcaíno, J. A., Csordas, A., del-Toro, N., Dianes, J. A., Griss, J., Lavidas, I., Mayer, G., Perez-Riverol, Y., Reisinger, F., Ternent, T., et al. (2016b) 2016 update of the PRIDE database and its related tools. Nucleic Acids Res, 44(D1), D447-56.
Vuppalanchi, D., Merianda, T. T., Donnelly, C., Pacheco, A., Williams, G., Yoo, S., Ratan, R. R., Willis, D. E. & Twiss, J. L. (2012) Lysophosphatidic acid differentially regulates axonal mRNA translation through 5'UTR elements. Mol Cell Neurosci, 50(2), 136-46.
Webb, B. L. & Proud, C. G. (1997) Eukaryotic initiation factor 2B (eIF2B). Int J Biochem Cell Biol, 29(10), 1127-31.
Welsh, G. I., Miller, C. M., Loughlin, A. J., Price, N. T. & Proud, C. G. (1998) Regulation of eukaryotic initiation factor eIF2B: glycogen synthase kinase-3 phosphorylates a conserved serine which undergoes dephosphorylation in response to insulin. FEBS Lett, 421(2), 125-30.
Wong, H. H., Lin, J. Q., Ströhl, F., Roque, C. G., Cioni, J. M., Cagnetta, R., Turner-Bridger, B., Laine, R. F., Harris, W. A., Kaminski, C. F. & Holt, C. E. (2017) RNA docking and local translation regulate site-specific axon remodeling in vivo. Neuron, 95(4), 852-868.e8.
Woo, C. W., Kutzler, L., Kimball, S. R. & Tabas, I. (2012) Toll-like receptor activation suppresses ER stress factor CHOP and translation inhibition through activation of eIF2B. Nat Cell Biol, 14(2), 192-200.
Wu, Y., Whiteus, C., Xu, C. S., Hayworth, K. J., Weinberg, R. J., Hess, H. F. & De Camilli, P. (2017) Contacts between the endoplasmic reticulum and other membranes in neurons. Proc Natl Acad Sci U S A, 114(24), E4859-E4867.
Yang, L., Sha, H., Davisson, R. L. & Qi, L. (2013) Phenformin activates the unfolded protein response in an AMP-activated protein kinase (AMPK)-dependent manner. J Biol Chem, 288(19), 13631-8.
Yoon, B. C., Jung, H., Dwivedy, A., O'Hare, C. M., Zivraj, K. H. and Holt, C. E. (2012) Local translation of extranuclear lamin B promotes axon maintenance, Cell, 148(4), 752-64.
Zivraj, K. H., Tung, Y. C., Piper, M., Gumy, L., Fawcett, J. W., Yeo, G. S. and Holt, C. E. (2010) Subcellular profiling reveals distinct and developmentally regulated repertoire of growth cone mRNAs, J Neurosci, 30(46), 15464-78.

FIGURE AND TABLE LEGENDS

Figure 1. eIF2α phosphorylation underlies Sema3A-induced upregulation of axonal protein synthesis. (A-B) Growth cones were treated with Tg (15 min) or Sema3A (10 min) and IF for total-eIF2α and p-eIF2α was measured (Unpaired t-test). **(C-D)** Growth cones were incubated with puromycin and co-treated with Tg (15 min) or Sema3A (10 min) and ISRIB, and IF for puromycin was measured (one-way ANOVA with Bonferroni's Multiple Comparison test). Error bars s.e.m. Scale bars 5 μm. See also Figure S1.

Figure 2. pSILAC-SP3 reveals 75 nascent proteins regulated by the Sema3A-p-eIF2α

pathway. (A) Schematic of pSILAC-SP3 methodology applied to somaless retinal axons. **(B)** Subset of NSPs regulated in response to Sema3A by p-eIF2α. Only significant NSP changes are shown (blue = downregulation, red = upregulation; p-value < 0.01). **(C)** KEGG pathway analysis (red = upregulated pathway, blue = downregulated pathway; cut-off ≥ 2 proteins per pathway). **(D)** Network-based cluster analysis of the enriched NSP changes induced by Sema3A-p-eIF2α signaling and their associated functional classes (blue nodes = downregulated NSPs, red nodes = upregulated NSPs, light blue edges = interactions known from databases, purple edges = interactions experimentally determined; green stars = NSPs belonging to the 'Response to stress' category; FDR < 0.05). (**E-F**) Validation of up-/down-regulated protein changes detected. Axons were pre-incubated with ISRIB for 30 min, co-stimulated with Sema3A for 15 min and IF for the protein of interest was quantified (One-way ANOVA with Bonferroni's Multiple Comparison test). **(G)** Correlation analysis of pSILAC- and qIF-derived detection of protein changes (r = 0.92). Error bars s.e.m. Scale bar 5 μm. See also Figure S2 and Table S1.

Figure 3. Sema3A-induced initial wave of local protein synthesis elicits eIF2α phosphorylation via PERK. (A) Retinal axons were immunostained for PERK, HRI and PKR. **(B-C)** Growth cones were co-treated with Sema3A and CHX, PP242 or U0126 for 10 min, and IF for total-eIF2α and p-eIF2α was measured (one-way ANOVA with Bonferroni's Multiple Comparison test). **(D-E)** Growth cones were co-treated with Sema3A and GSK2606414 (GSK) for 10 min, and IF for p-eIF2α was measured (one-way ANOVA with Bonferroni's Multiple Comparison test). **(F-G)** Growth cones were incubated with puromycin and co-treated with Sema3A and GSK for 10 min, and IF for puromycin was measured (one-way ANOVA with Bonferroni's Multiple Comparison test). **(H-I)** Growth cones of embryos injected with CoMO or PERK MO were incubated with puromycin and Sema3A for 10 min, and IF for puromycin was measured (one-way ANOVA with Bonferroni's Multiple Comparison test). Error bars s.e.m. Scale bars 5 μm. See also Figure S3.

Figure 4. Sema3A and canonical UPR signaling differentially control translation by distinct modulation of eIF2B. (A-B) Growth cones were co-treated with Sema3A and CHX (10 min), or Tg (15 min), and IF for eIF2Bε was measured (one-way ANOVA with Bonferroni's Multiple Comparison test). **(C)** RT-PCR for Actb (positive control; Turner-Bridger et al., 2018), Brn3a (negative control; Yoon et al. 2012) and eIF2Bε mRNAs. **(D-E)** Growth cones were co-treated with Sema3A and Tautomycin (TM) or U0126 (10 min), or treated with Tg (15 min), and IF for p-eIF2Bε (Ser539) was measured (one-way ANOVA with Bonferroni's Multiple Comparison test). **(F-G)** Growth cones were co-incubated with puromycin, Sema3A and TM for 10 min, and IF for puromycin was measured (one-way ANOVA with Bonferroni's Multiple Comparison test). **(H-I)** Intact brains of embryos stage 35/36 were incubated with TM for 30 min, NSPs were puromycilated over the last 15 min of the treatment, anti-puromycin WB was carried out and puromycin signal intensity was measured (Unpaired t-test). Error bars s.e.m. Scale bars 5 μm. See also Figure S4.

Figure 5. Spatially polarized phosphorylation of eIF2α mediates Sema3A-induced chemorepulsion. (A) Turning assay - arrow indicates the position of the pipette. **(B)** Cumulative distribution of turning assay outcome. A polarized gradient of Sema3A was generated and ISRIB, GSK or TM were bath-applied. Positive values indicate attraction, negative values indicate repulsion (Unpaired t-test). **(C)** Turning assay with somaless axons - arrow indicates the position of the pipette. Eye explants were removed immediately prior the experiment. **(D)** Cumulative distribution of turning assay outcome. A polarized gradient of Sema3A was generated and ISRIB was bath-applied. Positive values indicate attraction, negative values indicate repulsion (Unpaired t-test). **(E)** Growth cone immunostained for p-eIF2α with a line dividing the near/far sides. Arrow indicates the 90° polarized gradient of Sema3A. **(F)** Cumulative distribution assessing asymmetric increase of p-eIF2α by near/far ratio method (Unpaired t-test). **(G)** Asymmetric increase of p-eIF2α assessed by center of mass method (Unpaired t-test). **(H)** Sema3A-induced repulsive growth cone model – p-eIF2α

increases on the near-stimulus side, controlling β-actin polarized decrease (Cagnetta et al., 2018), thus helping asymmetric cytoskeleton deconstruction and filopodia collapse. Error bars s.e.m. Scale bar 5 μm. See also Figure S5.

Figure 6. PERK signaling is required for visual pathway development *in vivo*.

(A) Experimental outline to investigate the contribution of axonal PERK in RGCs only and Slit1 in the optic tract pathway substrate. Unilateral MO injection leads to a targeted KD in half of the nervous system. **(B)** Schematic of axons navigating the optic tract and reaching the tectum. TPB, Tectal Posterior Boundary; TAB, Tectal Anterior Boundary; TPA Tectal Projection Angle; MDT, Mid-Diencephalic Turn; A, Anterior; P, posterior; OC, Optic Chiasm; Tec, tectum; Di, Diencephalon; Hy, Hypothalamus; Tel, Telencephalon. **(C-G)** DiI-filled stage 41 retinotectal projections (Ax, Axon; Br, Brain). **(H)** Cumulative distribution of MDT angle measurements in unilateral KD of PERK in the axons or Slit1 in the optic tract substrate, or both (one-way ANOVA with Bonferroni's Multiple Comparison test). **(I)** Penetrance for MDT angles < 45° (Fisher's exact test). **(J)** Cumulative distribution of TPA measurements in unilateral KD of PERK in the axons or Slit1 in the optic tract substrate, or both. Positive values indicate angles pointing towards the TPB, negative values indicate angles pointing towards the TAB (one-way ANOVA with Bonferroni's Multiple Comparison test). **(K)** Penetrance of posterior tectum avoidance was measured as TPA < mean TPA in CoMO (i.e. -8.6°) (Fisher's exact test). **(L)** Single RGC axons in the tectum and line drawings of the corresponding trajectories shown by color-coded branch order: white = axon shaft, branches: red = primary, blue = secondary, yellow = tertiary. **(M)** Number of axon branches in the various orders and total number of branches in the PERK morphants (two-way ANOVA). **(N)** Length of axon branches in the PERK morphants (Unpaired t-test). **(O)** Formulation of Axon Complexity Index (ACI). Color indicates the branch order as in (L). **(P)** ACI in the PERK morphants (Fisher's exact test). Error bars s.e.m. Scale bar 100 μm (Figure 5C-G), 20 μm (Figure 5L). See also Figure S6.

Figure 7. eIF2Bε constitutes a pivotal node between the responses to canonical stress and Sema3A. Sema3A induces an initial (≤ 5 min) wave of local translation independent of the eIF2 pathway mediated by ERK-1/2 and mTOR. Simultaneously, eIF2Bε is locally translated in an ERK-1/2-mTOR-independent manner. The rapid increase in local protein synthesis triggers eIF2α phosphorylation via PERK at 10 min stimulation. Within this timecourse, ERK-1/2 represses GSK-3β and activates PP1, thus dephosphorylating eIF2Bε and increasing eIF2B activity. The engagement of p-eIF2α and increased eIF2B GEF activity generates a specific level of ternary complex higher than in the canonical stress response, resulting in the uORF-independent selective translation of 75 NSPs, upregulating global translation.
+p = phosphorylation, -p = dephosphorylation, ↑ and ↓= axonal translation upregulation and downregulation, dashed lines = indirect activation following rise in local protein synthesis, dotted lines = interaction, dashed circles = timing.

STAR METHODS

CONTACT FOR REAGENT AND RESOURCE SHARING

Further information and requests for resources and reagents should be directed to and will be fulfilled by the lead contact Christine E. Holt (ceh33@cam.ac.uk).

EXPERIMENTAL MODEL AND SUBJECT DETAILS

Xenopus laevis embryos maintenance

Xenopus laevis embryos of either sex were obtained by *in vitro* fertilization as previously described (Campbell and Holt, 2001), raised in 0.1x modified Barth's saline (MBS; 8.8 mM NaCl, 0.1 mM KCl, 0.24 mM $NaHCO_3$, 0.1 mM HEPES, 82 μM $MgSO_4$, 33 μM $Ca(NO_3)_2$, 41 μM $CaCl_2$) at 14–22°C and staged according to Nieuwkoop and Faber (1994). This research has been regulated under the Animals (Scientific Procedures) Act 1986 Amendment Regulations 2012 following ethical review by the University of Cambridge Animal Welfare and Ethical Review Body (AWERB).

METHOD DETAILS

Retinal explant cultures and axotomy assay on transwell filter

Whole eyes of anesthetized stage 35/36 embryos were dissected out and cultured at 20°C for 24h in 60% L15 minimal medium (Invitrogen), 1x Penicillin Streptomycin Fungizone on glass bottom dishes (MatTek) or on the top compartment of 6-well hanging inserts (Boyden chambers) with 1µm membrane pores (Falcon), coated on both sides of the membrane with poly-L-lysine (10 µg/ml, Sigma) and only on the bottom side with laminin (10 µg/ml, Sigma). For the pSILAC experiment 100 eye explants were cultured per condition, as detailed in Cagnetta et al., 2018. After 24 h, eye explants were pre-incubated with ISRIB for 30 min. Subsequently, eye explants were removed, scraped and washed off 7 times from the top compartment of the filter, leaving the somaless axons (~2µg protein typical yield) at the bottom. Sema3A or Sema3A and ISRIB were added, together with respective stable isotope-coded amino acids, to the somaless axons for 15 min. After stimulation the membrane was cut away, rinsed with ice cold PBS and lysed for protein extraction.

Pharmacological treatments

Stimulations were carried out using the following concentrations: Sema3A (150 ng/ml), Slit1 (200 ng/ml), ISRIB (200 nM), Thapsigargin (500 nM), Dithiothreitol (1 mM), GSK2606414 (300 nM), Cycloheximide (50 µM), PP242 (2.5 µM), U0126 (10 µM), Tautomycin (4nM).

Pulsed Stable Isotope Labelling by Amino acids in Cell culture

Experiments were performed in three independent biological replicates. Retinal explants were cultured in SILAC *light* medium (Lys0, Arg0) for 24 h and incubated in depletion medium (-Lys, -Arg) for 60 min prior pulse labeling. Subsequently, cell bodies were removed and somaless axons were incubated for 15 min with *medium* (M) (Lys4, Arg6) or *heavy* (H) isotope-coded amino acids (Lys8, Arg10). At 15 min samples were lysed, immediately pooled and processed by SP3.

Single-Pot Solid-Phase-enhanced Sample Preparation

Axons were harvested by the addition of lysis buffer (1% SDC, 0.1% SDS, 100mM TrisHCl ph 8.5, 10mM DTT, 1x protease inhibitor EDTA free). Samples were supplemented with 25 units Benzonase nuclease (Merck), and lysed in a Bioruptor (Diagenode) for 5 minutes (cycle 30/30, 4°C). Alkylation was performed by addition of 30 mM Chloroacetamide followed by incubation in the dark for 30 min. Protein clean-up, digestion and peptide clean-up were performed using a modified version of the recently developed ultrasensitive sample preparation protocol SP3 (Hughes et al., 2014). In brief, 5 µL of beads (1:1 mixture of hydrophilic and hydrophobic SeraMag Carboxylate-Modified beads, GE Life Sciences) were added to each sample. Acidified acetonitrile was added to achieve a final fraction of organic solvent of 50%. Beads were incubated for 10 min to allow complete binding of proteins to the beads. Protein clean-up was performed by subsequent wash with 70% Ethanol and once with Acetonitrile. For digestion, 0.1 µg sequencing grade Trypsin/LysC (Promega) was added and digestion was performed at 37°C for 16 h. Peptides were eluted with 9 µL 5% DMSO. 1 µL 10% formic acid was added and samples were stored at -20°C prior to MS analysis.

Mass Spectrometry

Samples were analyzed on a Orbitrap Velos Pro mass spectrometer (Thermo Scientific) using default settings. The mass spectrometer was coupled to a UPLC systems (Waters nanoAcquity UPLC). Peptides were loaded onto trap columns (Waters nanoAcquity Symmetry C_{18}, 5 µm, 180 µm × 20 mm) with Buffer A (0.1% formic acid in water) and separated over a 25 cm analytical column (Acclaim PepMap RSLC, 75 µm × 2 µm) using 240 minute linear gradients from 3-40% Buffer B (0.1% formic acid in Acetonitrile). MS2 Fragmentation was set to CID, and MSMS scans were acquired in the ion trap.

Proteomics data processing

Raw data were processed with Maxquant (version 1.4.1.2) (Cox and Mann, 2008) using default settings. MSMS spectra were searched against the *Xenopus laevis* Uniprot database

(v20140925) concatenated to a database containing protein sequences of common contaminants. Raw data from Cagnetta et al., 2018 was used as a library to increase depth of identifications using the match-between-runs option, which was enabled in Maxquant. Enzyme specificity was set to trypsin/P, allowing a maximum of two missed cleavages. Cysteine carbamidomethylation was set as fixed modification, and methionine oxidation and protein N-terminal acetylation were used as variable modifications. The minimal peptide length was set to six amino acids. The mass tolerances were set to 20 ppm for the first search, and 4.5 ppm for the main search. Global false discovery rates for peptide and protein identification were set to 1%. The match-between-runs and re-quantify options were enabled.

Immunocytochemistry

Retinal cultures were fixed by paraformaldehyde except for anti-β-actin (AC-15 FITC) and anti-Gsn where methanol fixation was carried out. Secondary antibodies were species-specific dye-conjugated (Alexa Fluor, Invitrogen).

Puromycilation of NSPs

Retinal cultures were incubated with puromycin (2 ng/µl) for the condition and time (up to 15 min) of interest, fixed and incubated with anti-puromycin Alexa Fluor conjugate antibody. Intact brains were incubated with puromycin (5 ng/µl) for 15 min in the condition of interest (Control or Tautomycin (20nM)), rinsed in culture medium, lysed and western blot anti-puromycin was carried out.

Puromycilation of NSPs and Proximity Ligation Assay

Retinal cultures were incubated with puromycin (2 ng/µl) for 10 min in the condition of interest, fixed and incubated with anti-puromycin and anti-Atf4 antibodies. Subsequently, Proximity Ligation Assay (PLA) was carried out using species-specific probes (tom Dieck et al., 2015).

Reverse Transcription Polymerase Chain Reaction

RNA was extracted from using RNAqueous-Micro Total RNA Isolation Kit. Primers were designed using *Primer3Plus* software. The annealing temperature used was 58°C for β-actin and Brn3a, 67°C for eIF2Bε.

Growth cone turning assay

Retinal explants from stage 35/36 embryos were cultured for 14-18 h on coverslips coated with poly-L-lysine (10 µg/ml) and laminin (10 µg/ml). Gradients of Sema3A (9 µg/ml) or control were generated by pulsatile ejection as described previously (Lohof et al., 1992; Campbell and Holt, 2001) for 60 min placing the micropipette at a starting distance equal to 100 µm and at an angle of 45° relative to the initial direction of the axon shaft. ISRIB (200 nM), GSK2606414 (300 nM), or Tautomycin (4nM) were bath-applied immediately prior to the start of the gradient assay.

For growth cone gradient assay the gradient was generated for 10 min placing the micropipette at 70 µm distance and at an angle of 90° relative to the growth cone and the initial direction of the axon shaft (Cagnetta et al., 2018). Subsequently samples were immediately fixed and immunostained for p-eIF2α.

Blastomere injection

Xenopus embryos were injected at the 4-cell stage in the dorsal animal blastomeres as previously described (Roque et al., 2016). 18 ng of PERK/Slit1/Control MO were injected into the blastomere of interest (Figure 6A).

DiI anterograde axon labeling

Stage 41 embryos were fixed in 4% formaldehyde in PBS at 4°C overnight. DiI solution was prepared by dissolving DiI powder (Thermo Scientific) in ethanol and injected into the eye cavity until completely filled. The embryos were incubated at room temperature for 48h to ensure complete dye diffusion. The brain was dissected and mounted in 1xPBS. The

contralateral brain hemisphere was imaged.

Exposed brains

Stage 33/34 embryo brains were exposed by removing the overlying eye and epidermis (Wong et al., 2017) to ISRIB (2 µM) treatment at 22°C overnight, fixed and DiI injection was carried out.

Electroporation

Target eye electroporation was performed as previously described (Wong et al., 2017). The eye primordia of embryos stage 28 were injected with electroporation mixture (1 µg/µl pCS2+mGFP and 0.5 mM Control MO/PERK MO), followed by electric pulses of 50 ms duration at 1000 ms intervals, delivered at 18 V. The embryos were raised in 0.1x MBS until stage 45.

Western blot

Puromycilation assay of brains of stage 35/36 embryos and MOs specificity test on brain and eye tissue were carried out by western blot. Pierce BCA Protein Assay kit (Thermo Fisher Scientific) and spectrophotometry were used to determine the sample concentration. Bovine albumin serum (BSA, Invitrogen) was used to create a standard curve for protein concentration and for normalizing the concentration among samples. The antibody of interest was incubated at 4°C overnight in 5% BSA solution for the anti-Slit1 antibody, or 5% milk solution for the anti-puromycin and anti-PERK antibodies. The blots were then incubated with HRP-conjugated secondary antibodies (Abcam) at room temperature for 45 min, followed by ECL-based detection (Invitrogen).

QUANTIFICATION AND STATISTICAL ANALYSIS

Statistics

Data were analyzed with PRISM 5 (GraphPad). Data are presented as mean and error bars represent s.e.m. Experiments were performed in at least three independent biological replicates. Details of statistical tests used and p-values are presented in the figure legends. *p≤0.05, **p≤0.01, ***p≤0.001, ****p≤0.0001, ns: non-significant.

Bioinformatic data analysis

For protein quantification a minimum ratio count of 2 was set. The iBAQ was calculated to determine relative abundance levels of the pre-existing light-labeled proteins. Protein ratios were log2-transformed using the Perseus computational framework, and H/M ratios of NSPs were normalized to the median to center the distribution of ratios at 0 on the log2 scale, i.e. comparable numbers of proteins are up-regulated and down-regulated, respectively. To test whether the log2 ratio of each protein was significantly different from zero, p-values were computed by a moderated t-test implemented in the R/Bioconductor package limma (Ritchie et al., 2015). p-values were corrected for multiple testing by controlling the false discovery rate with the method of Benjamini-Hochberg. Enrichment of categorical annotations (Gene Ontology) was determined using DAVID. Pathway and disease analyses were carried out using KEGG. Interaction network analysis was obtained by employing String v10.5 database. Each node represents a NSP change and each edge shows protein-protein interaction, disconnected nodes are not shown for simplicity. Upstream regulator analyses were carried out based on previous datasets identifying the targets of the following translational regulators: Apc, Mena, Fmrp, Tdp43, Fus, mTOR, PERK and GCN2 (Preitner et al, 2014; Vidaki et al., 2017; Darnell et al, 2011; Colombrita et al., 2012; Thoreen et al., 2012; Dang do et al., 2009).

Quantification of Immunofluorescence

For the quantification of fluorescence intensity, isolated growth cones were selected randomly with phase optics. Low exposure was set up to avoid pixel saturation and the same gain and

exposure settings were used for digital capture of images for each experiment which was performed in the same day, except for the growth cone gradient assay where the IF of the near and far sides within the same growth cone were compared. The outline of each single growth cone was traced using the phase image to define the region of interest (ROI) and the mean pixel intensity per unit area was measured in each channel using *Volocity* software. The background fluorescence was measured in a ROI as close as possible to the growth cone selected and subtracted to the mean fluorescence value of the growth cone. In the figures brightness/contrast settings were adjusted equally across images collected in the same experiment for presentation clarity.

For the growth cone gradient assay IF ratio analysis, the growth cone was bisected into two areas by a line drawn through the axon shaft and the background fluorescence level was subtracted. For the center of mass analysis, measurement was calculated as the average of all pixel locations weighted as intensity by using *ImageJ* software. The center of mass of the bright field was subtracted from the center of mass of the fluorescence signal.

Turning assay measurement

Turning angles were measured on growth cone images taken at 0 and 60 min using *ImageJ* software.

DiI quantification

For optic tract width quantification ten equally spaced concentric circles (C1-C10) were overlaid on the tract images with the center of the circles overlying the optic chiasm (OC) and C10 overlaying the Tectal Posterior Boundary (TPB) (Figure S6A). The widths of C2-4 and C5-8, corresponding respectively to pre- and post-caudal turn, were averaged. Lastly, the pre- and post-turn widths were normalized to the brain size, defined by the distance between OC and TPB. Mid-diencephalic turn (MDT) was measured as the angle between the pre-turn axon bundle (drawing a line from the optic chiasm and the ventral side of the MDT) and the post-turn axon bundle (drawing a line from the ventral side of the MDT and the tip of the most pioneer

axon) (Figure 6B). The tectal projection angle (TPA) was measured as the angle between the post-turn tract and the most anteriorly projecting axon (Figure 6B). TPA was considered positive if pointing towards the posterior tectum, negative if pointing towards the anterior side of the tectum.

DATA AND SOFTWARE AVAILABILITY

Data availability

Table S1: Axonal NSP changes induced by the Sema3A-p-eIF2α pathway – Related to Figure 2, Figure S2 and Table S2. The accession number for the mass spectrometry proteomics data reported in this paper is ProteomeXchange Consortium via the PRIDE (Vizcaíno et al., 2016): PXD009250.

KEY RESOURCE TABLE

REAGENT or RESOURCE	SOURCE	IDENTIFIER
Antibodies		
anti-eIF2α	Abcam	Cat#ab137626; RRID:AB_2736873
anti-p-eIF2α	Abcam	Cat#ab32157; RRID:AB_732117
anti-puromycin Alexa Fluor 488 conjugate	Millipore	Cat#MABE343-AF488; RRID:AB_2736875
anti-puromycin Alexa Fluor 647 conjugate	Millipore	Cat#MABE343-AF647; RRID:AB_2736876
anti-puromycin	Millipore	Cat#MABE343; RRID:AB_2566826
anti-Actb	Abcam	Cat#ab6277; RRID:AB_305394
anti-Gsn	Proteintech	Cat#11644-2-AP; RRID:AB_2295090
anti-RpL7a	Abcam	Cat#ab155147; RRID:AB_2736874
anti-Atf4	Abcam	Cat# ab85049; RRID:AB_1861369
anti-eIF2Bε	Abcam	Cat#ab32713; RRID:AB_2230901
anti-p-eIF2Bε (Ser539)	Proteintech	N/A (customized)
anti-PERK	Cell signaling	Cat#3192; RRID:AB_2095847
anti-Tuba	Sigma	Cat#T6074; RRID:AB_477582
anti-Slit1	Abcam	Cat# ab115892; RRID:AB_10903854
Chemicals, Peptides, and Recombinant Proteins		
Sema3A	R&D Systems	Cat#1250-S3
Slit1	R&D Systems	Cat#6514-SL
ISRIB	Sigma	Cat#SML0843
Thapsigargin	Sigma	Cat#T9033
Dithiothreitol	Sigma	Cat#D0632
GSK2606414	Calbiochem	Cat#516535
Cycloheximide	Sigma	Cat#C4859
PP242	Tocris	Cat#4257
U0126	Tocris	Cat#1144
Tautomycin	Calbiochem	Cat#580551
Poly-L-lysine	Sigma	Cat#P1274
Laminin	Sigma	Cat#L2020
Leibovitz L-15 medium –Lys -Arg	Gibco Life Technologies	N/A (customized)
Stable isotope-coded amino acids Lys4	Silantes GmbH	Cat#211103913
Stable isotope-coded amino acids Lys8	Silantes GmbH	Cat#211603902
Stable isotope-coded amino acids Arg6	Silantes GmbH	Cat#201203902
Stable isotope-coded amino acids Arg10	Silantes GmbH	Cat#201603902
Puromycin	Sigma	Cat#P8833
Sera-Mag Speed Beads A	GE Healthcare	Cat#24152105050250
Sera-Mag Speed Beads B	GE Healthcare	Cat#44152105050250
Trypsin/LysC	Promega	Cat#V5071
Critical commercial assays		
RNAqueous-Micro Total RNA Isolation Kit	Invitrogen	Cat#AM1931
OneStep RT-PCR kit	QIAGEN	Cat#210210
Duolink *in situ* PLA kit	Sigma	Cat#DUO92014
Deposited data		
Proteomics data	This paper	PRIDE: PXD009250
Experimental Models: Organisms/Strains		
X. laevis	Nasco	https://www.enasco.com/product/LM00535MX/
Oligonucleotides		
Primer: β-actin *for* 5' CCTGTGCAGGAAGATCACAT 3' *rev* 5' TGTTAAAGAGAATGAGCCCC 3'	Sigma	N/A
Primer: Brn3a *for* 5' TGAGCGATTCAAGCAGAGGAGG 3' *rev* 5' TGCGACAGGGTGAGGGATTCAAAC 3'	Sigma	N/A
Primer: eIF2Bε *for* 5' TGATGATGCAGGCGCTGGAA 3' *rev 5'* CAGGTGAAGCAGGGTGGCTTTCTG 3'	Sigma	N/A
Morpholino: Control MO (CoMO) 5' CCTCTTACCTCAGTTACAATTTATA 3'	Gene Tools	N/A
Morpholino: PERK MO 5' CGAACACTTTCACCTCATAACACTT 3'	Gene Tools	N/A
Morpholino: Slit1 MO 5' AGTAGTCTCAATGACACAATGACCA 3'	Gene Tools	N/A
Software and Algorithms		
Volocity	v.6.3.1	RRID: SCR_002668
GraphPad PRISM	v.5.0c	RRID: SCR_002798
ImageJ	v.149	RRID:SCR_003070
DAVID	v.6.8	RRID:SCR_001881
KEGG	N/A	RRID:SCR_012773
String	v10.5	RRID:SCR_005223
Maxquant	v1.4.1.2	RRID:SCR_014485
Perseus	v1.5.1.6 or 1.5.5.3	RRID:SCR_015753

Figure 1

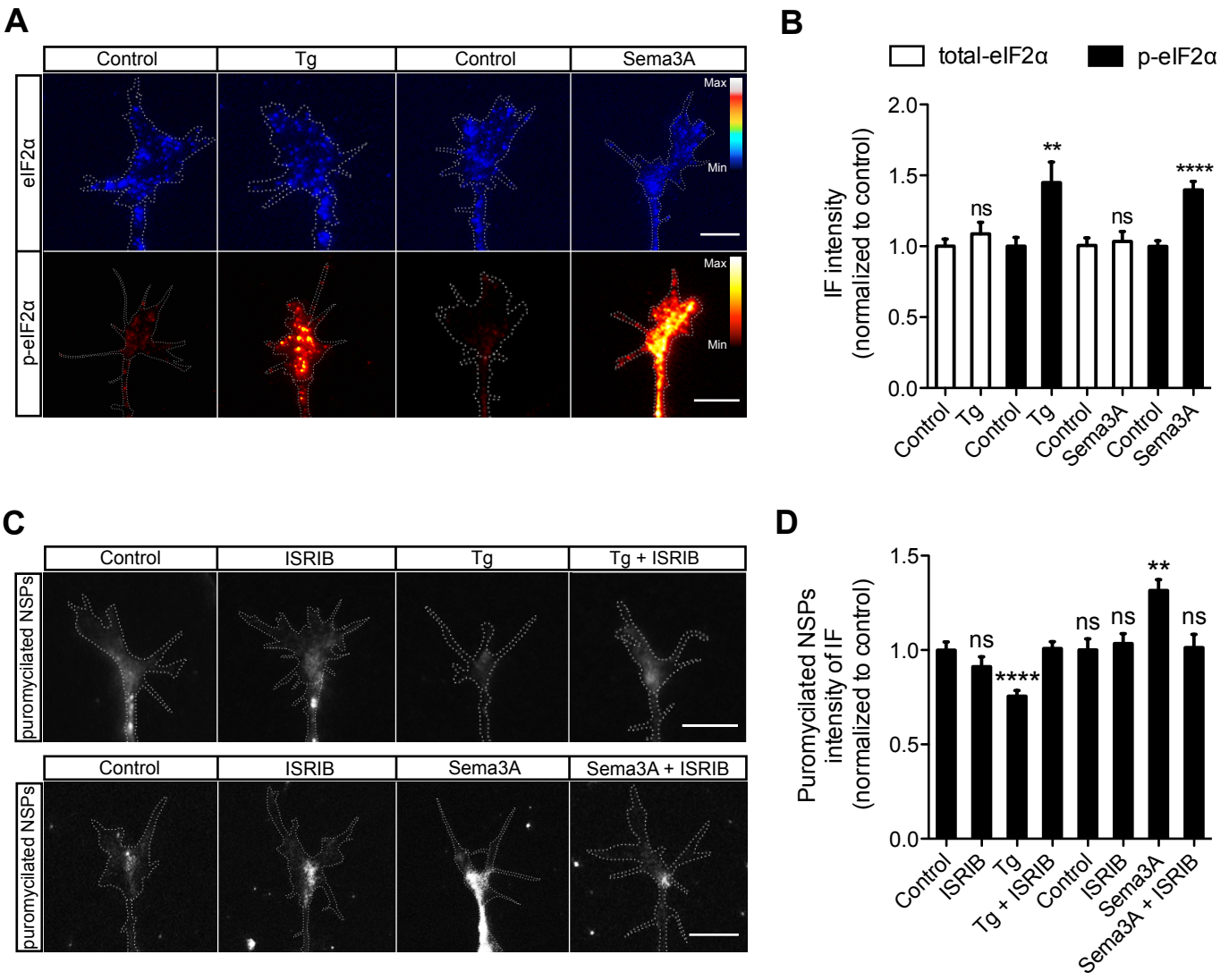
A
Control
Tg
Control
Sema3A
eIF2α
p-eIF2α
Max
Min
B
total-eIF2α
p-eIF2α
IF intensity
(normalized to control)
2.0
1.5
1.0
0.5
0.0
ns
**
ns
****
Control
Tg
Control
Tg
Control
Sema3A
Control
Sema3A
C
Control
ISRIB
Tg
Tg + ISRIB
puromycilated NSPs
Control
ISRIB
Sema3A
Sema3A + ISRIB
puromycilated NSPs
D
Puromycilated NSPs
intensity of IF
(normalized to control)
1.5
1.0
0.5
0.0
ns
****
ns
ns
**
ns
Control
ISRIB
Tg
Tg + ISRIB
Control
ISRIB
Sema3A
Sema3A + ISRIB

Figure 2

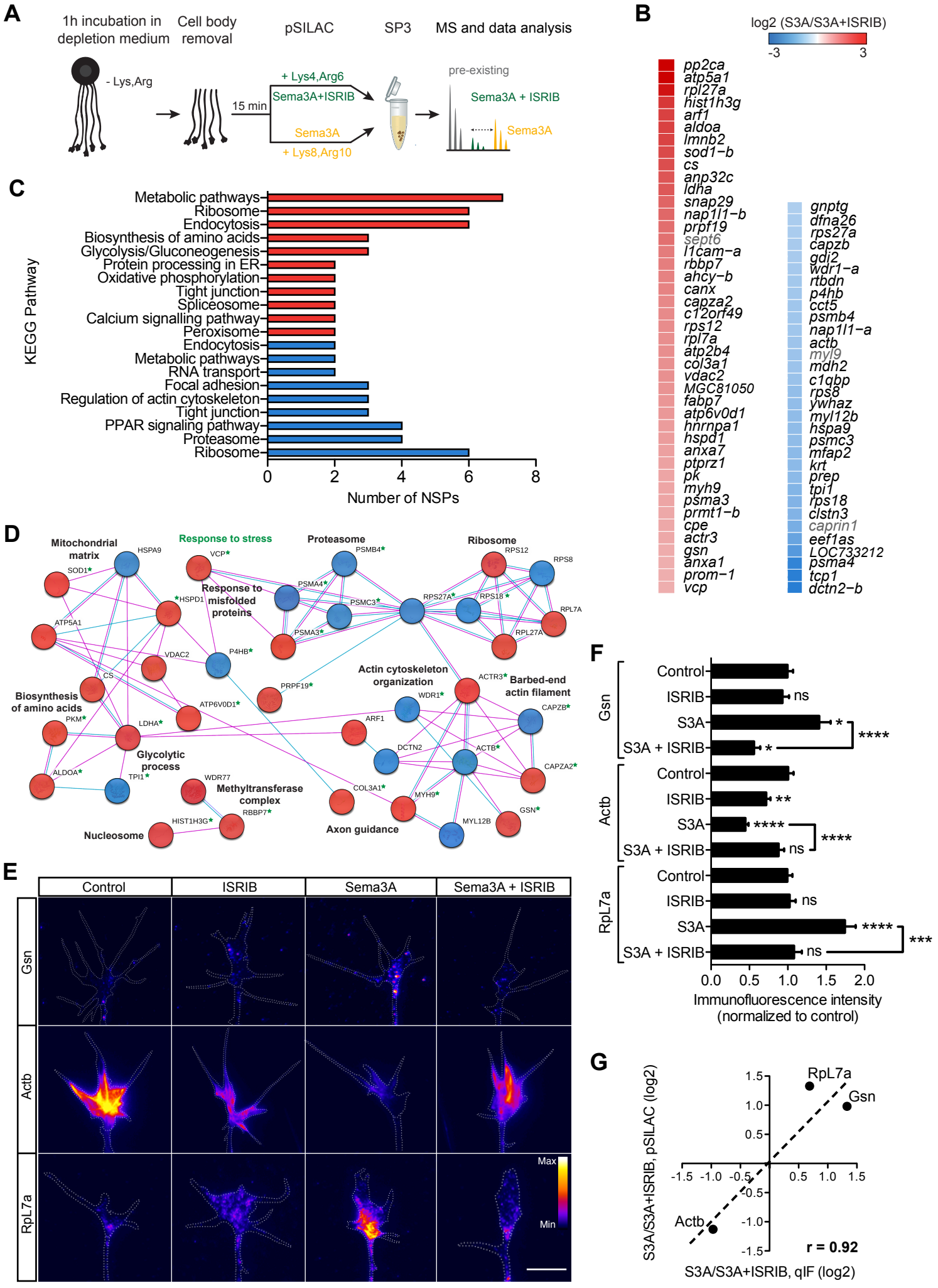
A
1h incubation in depletion medium
Cell body removal
pSILAC
SP3
MS and data analysis
- Lys,Arg
15 min
+ Lys4,Arg6
Sema3A+ISRIB
Sema3A
+ Lys8,Arg10
pre-existing
Sema3A + ISRIB
Sema3A
B
log2 (S3A/S3A+ISRIB)
-3
3
pp2ca
atp5a1
rpl27a
hist1h3g
arf1
aldoa
lmnb2
sod1−b
cs
anp32c
ldha
snap29
nap1l1−b
prpf19
sept6
l1cam−a
rbbp7
ahcy−b
canx
capza2
c12orf49
rps12
rpl7a
atp2b4
col3a1
vdac2
MGC81050
fabp7
atp6v0d1
hnrnpa1
hspd1
anxa7
ptprz1
pk
myh9
psma3
prmt1−b
cpe
actr3
gsn
anxa1
prom−1
vcp
gnptg
dfna26
rps27a
capzb
gdi2
wdr1−a
rtbdn
p4hb
cct5
psmb4
nap1l1−a
actb
myl9
mdh2
c1qbp
rps8
ywhaz
myl12b
hspa9
psmc3
mfap2
krt
prep
tpi1
rps18
clstn3
caprin1
eef1as
LOC733212
psma4
tcp1
dctn2−b
C
KEGG Pathway
Metabolic pathways
Ribosome
Endocytosis
Biosynthesis of amino acids
Glycolysis/Gluconeogenesis
Protein processing in ER
Oxidative phosphorylation
Tight junction
Spliceosome
Calcium signalling pathway
Peroxisome
Endocytosis
Metabolic pathways
RNA transport
Focal adhesion
Regulation of actin cytoskeleton
Tight junction
PPAR signaling pathway
Proteasome
Ribosome
0
2
4
6
8
Number of NSPs
D
Mitochondrial matrix
HSPA9
SOD1
ATP5A1
Response to stress
VCP
HSPD1
Response to misfolded proteins
Proteasome
PSMB4
PSMA4
PSMC3
PSMA3
Ribosome
RPS12
RPS8
RPS27A
RPS18
RPL7A
RPL27A
VDAC2
P4HB
CS
Biosynthesis of amino acids
PKM
LDHA
ATP6V0D1
PRPF19
Actin cytoskeleton organization
ACTR3
Barbed-end actin filament
WDR1
CAPZB
ARF1
DCTN2
ACTB
CAPZA2
Glycolytic process
ALDOA
TPI1
WDR77
Methyltransferase complex
RBBP7
HIST1H3G
Nucleosome
COL3A1
MYH9
MYL12B
GSN
Axon guidance
E
Control
ISRIB
Sema3A
Sema3A + ISRIB
Gsn
Actb
RpL7a
Max
Min
F
Gsn
Actb
RpL7a
Control
ISRIB
S3A
S3A + ISRIB
ns
*
****
**
***
0.0
0.5
1.0
1.5
2.0
Immunofluorescence intensity (normalized to control)
G
RpL7a
Gsn
Actb
1.5
1.0
0.5
-1.5
-1.0
-0.5
r = 0.92
S3A/S3A+ISRIB, pSILAC (log2)
S3A/S3A+ISRIB, qIF (log2)

Figure 3

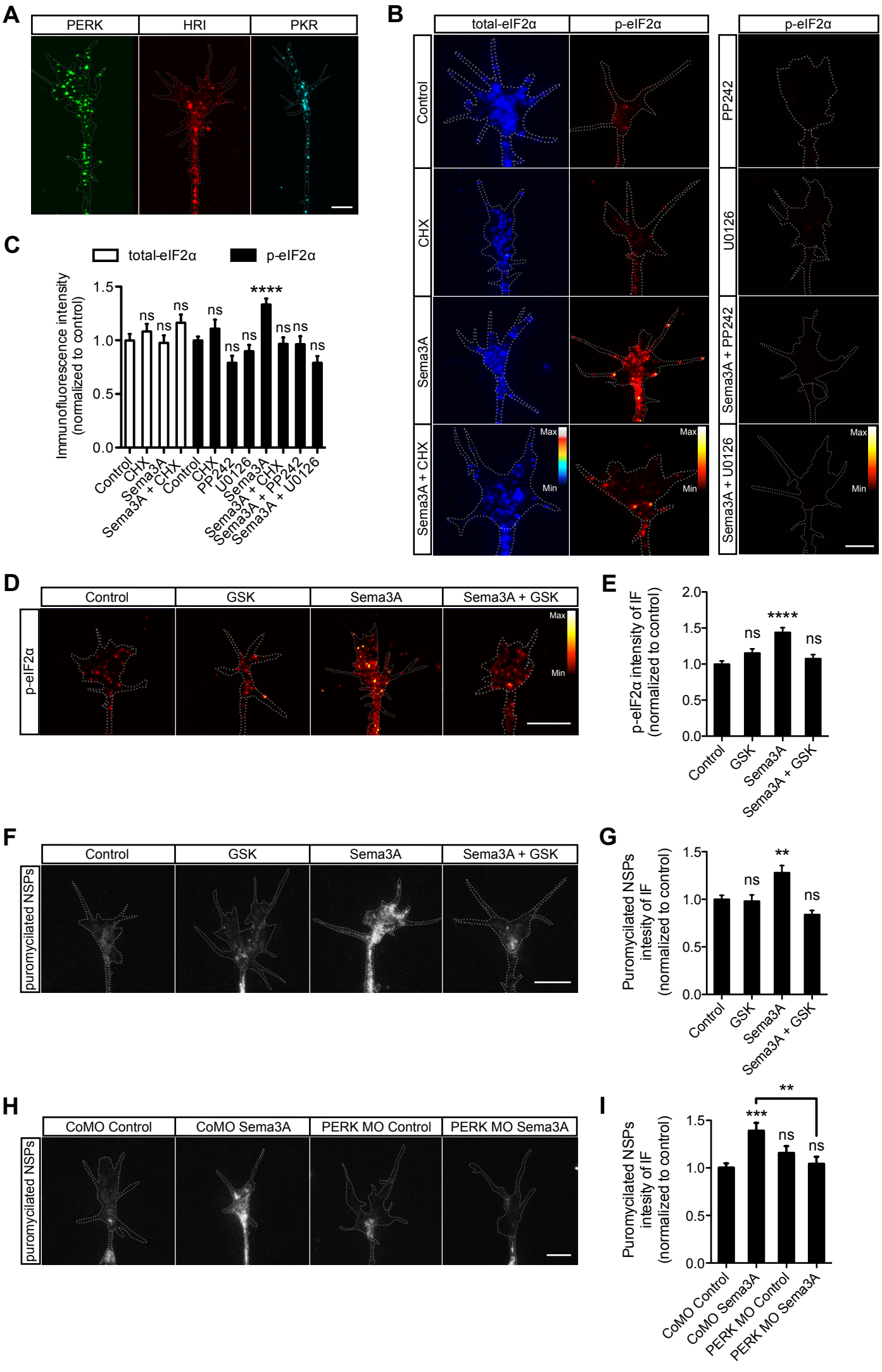
A
PERK
HRI
PKR
B
total-eIF2α
p-eIF2α
p-eIF2α
Control
CHX
Sema3A
Sema3A + CHX
PP242
U0126
Sema3A + PP242
Sema3A + U0126
Max
Min
C
total-eIF2α
p-eIF2α
Immunofluorescence intensity (normalized to control)
1.5
1.0
0.5
0.0
ns
****
Control
CHX
Sema3A
Sema3A + CHX
PP242
U0126
Sema3A + PP242
Sema3A + U0126
D
Control
GSK
Sema3A
Sema3A + GSK
p-eIF2α
Max
Min
E
p-eIF2α intensity of IF (normalized to control)
2.0
1.5
1.0
0.5
0.0
ns
****
Control
GSK
Sema3A
Sema3A + GSK
F
Control
GSK
Sema3A
Sema3A + GSK
puromycilated NSPs
G
Puromycilated NSPs intesity of IF (normalized to control)
1.5
1.0
0.5
0.0
ns
**
Control
GSK
Sema3A
Sema3A + GSK
H
CoMO Control
CoMO Sema3A
PERK MO Control
PERK MO Sema3A
puromycilated NSPs
I
Puromycilated NSPs intesity of IF (normalized to control)
1.5
1.0
0.5
0.0
***
ns
**
CoMO Control
CoMO Sema3A
PERK MO Control
PERK MO Sema3A

Figure 4

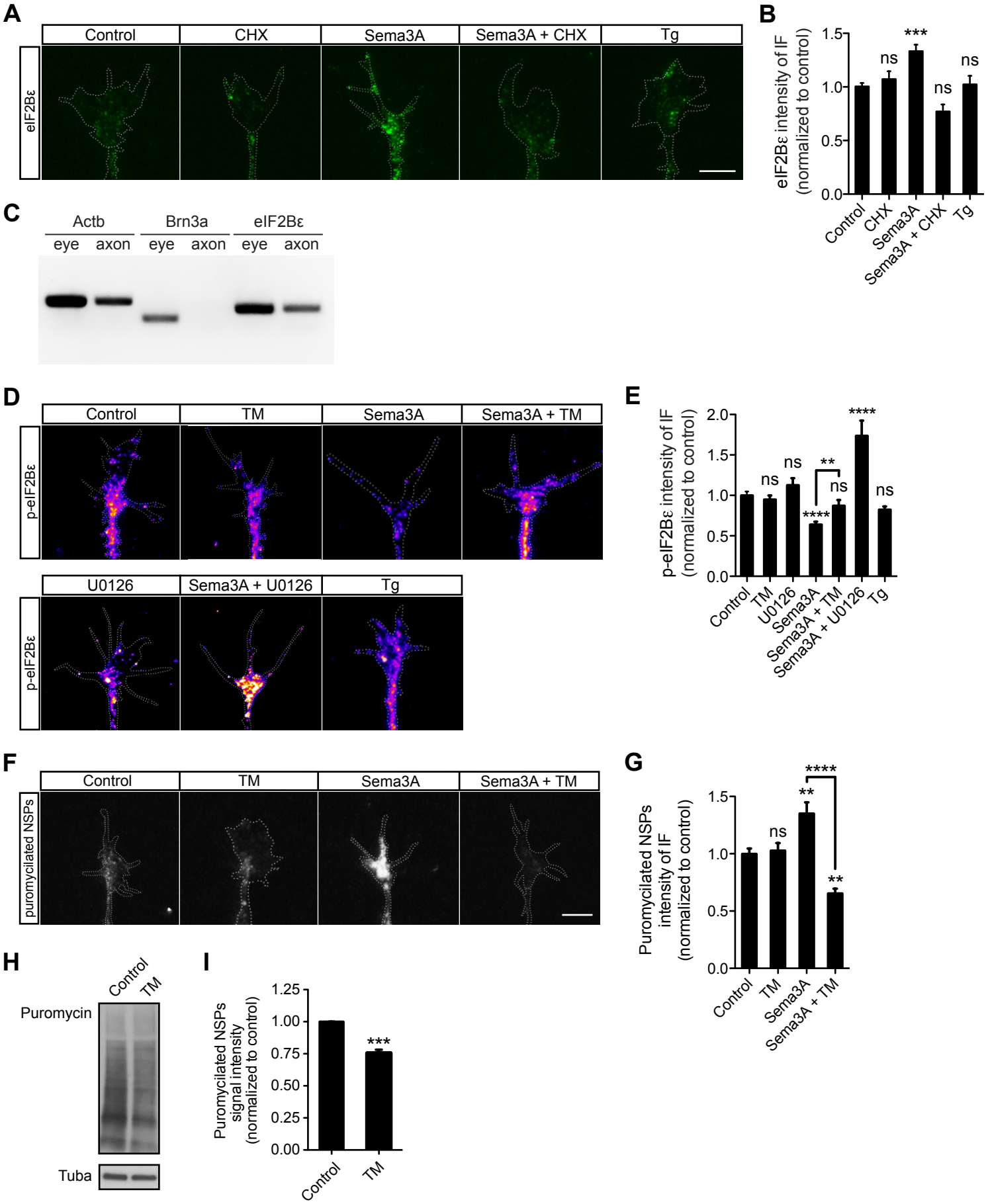
A
Control
CHX
Sema3A
Sema3A + CHX
Tg
eIF2Bε
B
eIF2Bε intensity of IF (normalized to control)
1.5
1.0
0.5
0.0
***
ns
ns
ns
Control
CHX
Sema3A
Sema3A + CHX
Tg
C
Actb
Brn3a
eIF2Bε
eye
axon
eye
axon
eye
axon
D
Control
TM
Sema3A
Sema3A + TM
p-eIF2Bε
U0126
Sema3A + U0126
Tg
p-eIF2Bε
E
p-eIF2Bε intensity of IF (normalized to control)
2.0
1.5
1.0
0.5
0.0
****
ns
ns
**
****
ns
ns
Control
TM
U0126
Sema3A
Sema3A + TM
Sema3A + U0126
Tg
F
Control
TM
Sema3A
Sema3A + TM
puromycilated NSPs
G
Puromycilated NSPs intensity of IF (normalized to control)
1.5
1.0
0.5
0.0
****
**
**
ns
Control
TM
Sema3A
Sema3A + TM
H
Control
TM
Puromycin
Tuba
I
Puromycilated NSPs signal intensity (normalized to control)
1.25
1.00
0.75
0.50
0.25
0.00
***
Control
TM

Figure 5

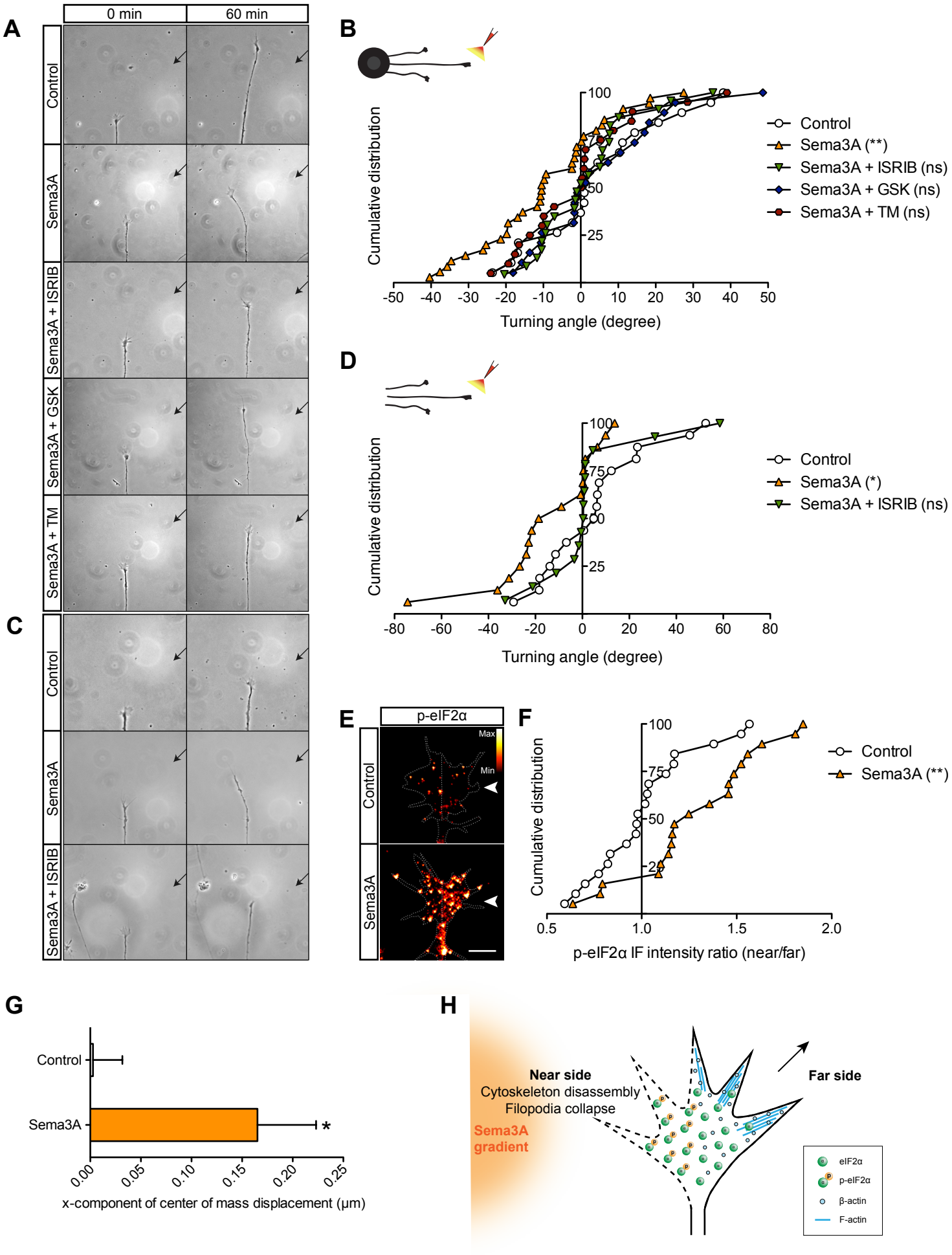
A
0 min
60 min
Control
Sema3A
Sema3A + ISRIB
Sema3A + GSK
Sema3A + TM
B
Cumulative distribution
Turning angle (degree)
Control
Sema3A (**)
Sema3A + ISRIB (ns)
Sema3A + GSK (ns)
Sema3A + TM (ns)
C
Control
Sema3A
Sema3A + ISRIB
D
Cumulative distribution
Turning angle (degree)
Control
Sema3A (*)
Sema3A + ISRIB (ns)
E
p-eIF2α
Max
Min
Control
Sema3A
F
Cumulative distribution
p-eIF2α IF intensity ratio (near/far)
Control
Sema3A (**)
G
Control
Sema3A
x-component of center of mass displacement (μm)
H
Near side
Cytoskeleton disassembly
Filopodia collapse
Sema3A gradient
Far side
eIF2α
p-eIF2α
β-actin
F-actin

Figure 6

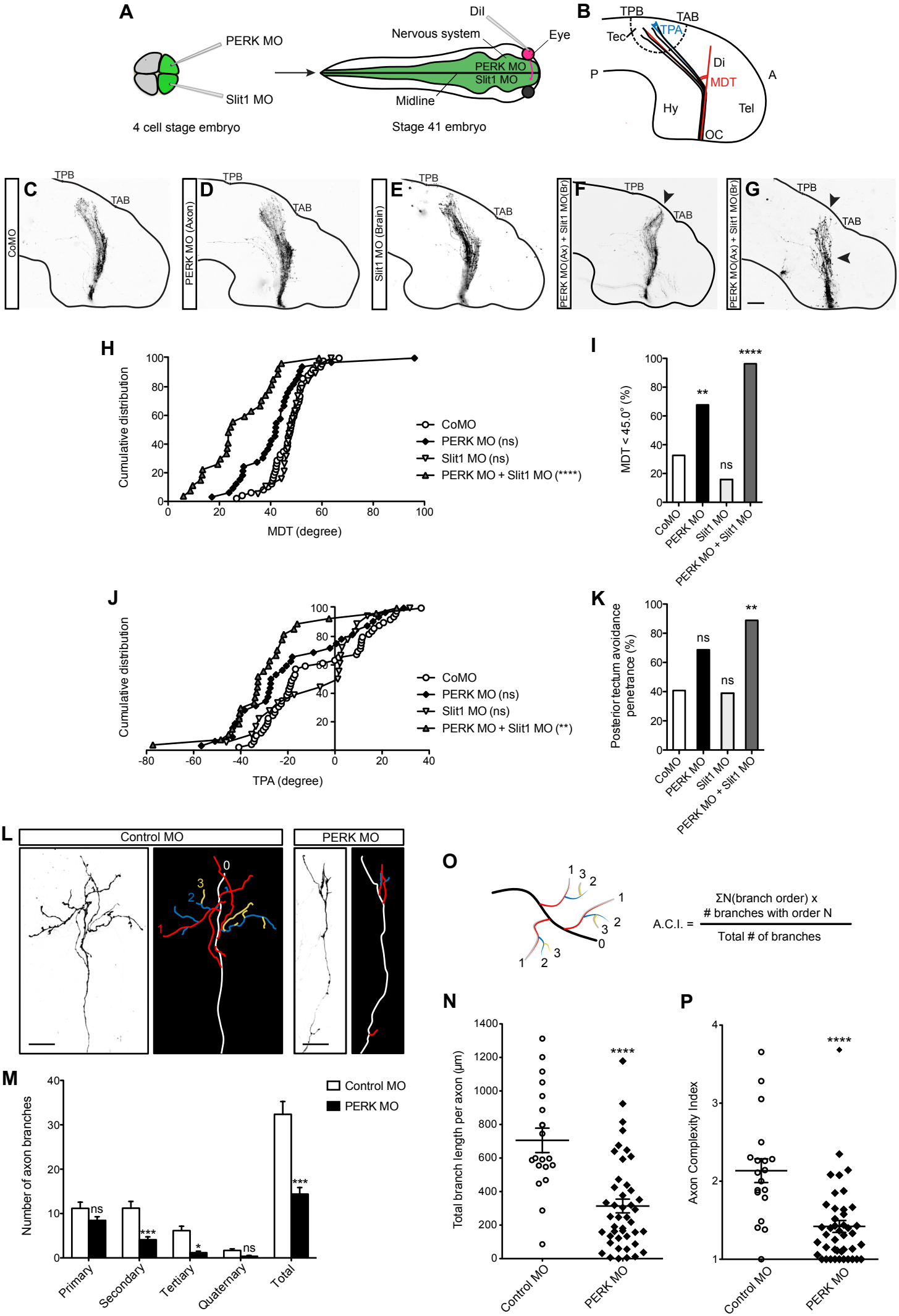
A
PERK MO
Slit1 MO
4 cell stage embryo
DiI
Nervous system
Eye
PERK MO
Slit1 MO
Midline
Stage 41 embryo
B
TPB
TAB
Tec
TPA
Di
MDT
P
A
Hy
Tel
OC
C
CoMO
D
PERK MO (Axon)
E
Slit1 MO (Brain)
F
PERK MO(Ax) + Slit1 MO(Br)
G
PERK MO(Ax) + Slit1 MO(Br)
H
Cumulative distribution
MDT (degree)
CoMO
PERK MO (ns)
Slit1 MO (ns)
PERK MO + Slit1 MO (****)
I
MDT < 45.0° (%)
**
ns
****
CoMO
PERK MO
Slit1 MO
PERK MO + Slit1 MO
J
Cumulative distribution
TPA (degree)
CoMO
PERK MO (ns)
Slit1 MO (ns)
PERK MO + Slit1 MO (**)
K
Posterior tectum avoidance penetrance (%)
ns
ns
**
CoMO
PERK MO
Slit1 MO
PERK MO + Slit1 MO
L
Control MO
PERK MO
M
Number of axon branches
Control MO
PERK MO
ns
***
*
ns
***
Primary
Secondary
Tertiary
Quaternary
Total
O
A.C.I. = ΣN(branch order) x # branches with order N / Total # of branches
N
Total branch length per axon (μm)
****
Control MO
PERK MO
P
Axon Complexity Index
****
Control MO
PERK MO

Figure 7

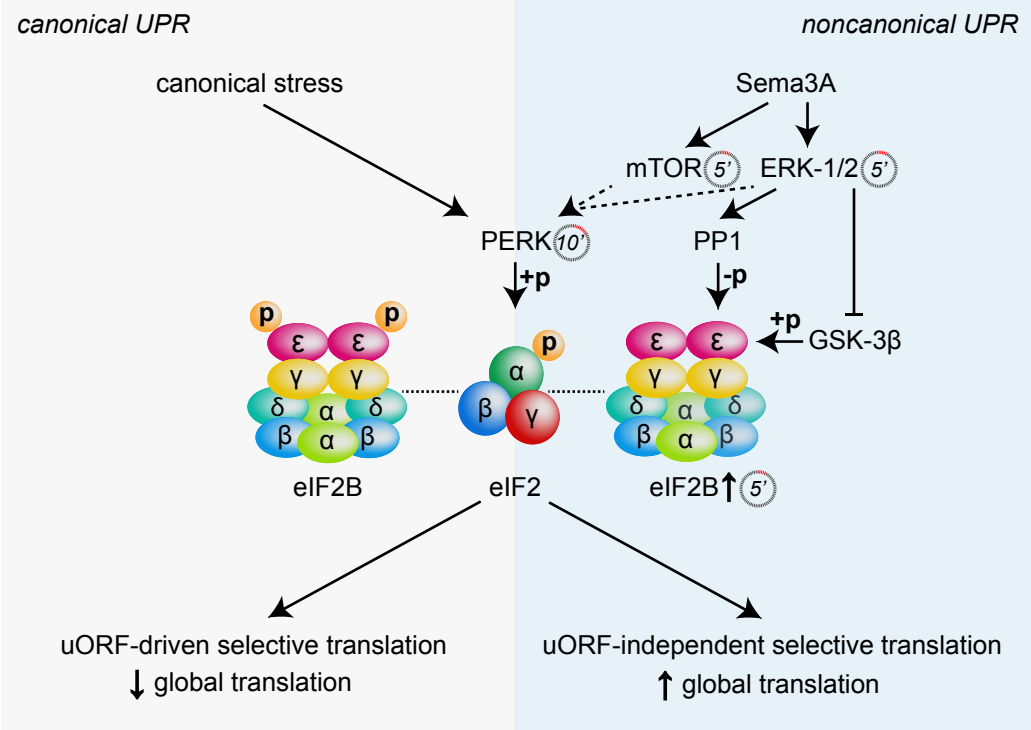
canonical UPR
noncanonical UPR
canonical stress
Sema3A
mTOR 5'
ERK-1/2 5'
PERK 10'
PP1
+p
-p
+p
GSK-3β
eIF2B
eIF2
eIF2B 5'
uORF-driven selective translation
↓ global translation
uORF-independent selective translation
↑ global translation

Figure S1

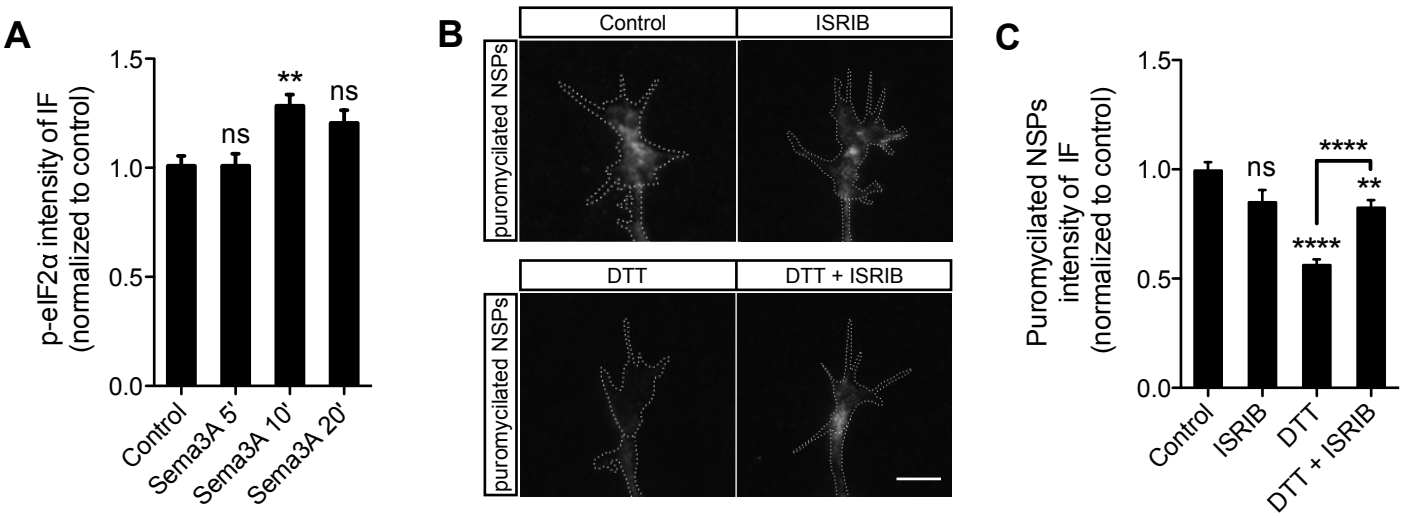
A
p-eIF2α intensity of IF (normalized to control)
1.5
1.0
0.5
0.0
ns
**
ns
Control
Sema3A 5'
Sema3A 10'
Sema3A 20'
B
Control
ISRIB
puromycilated NSPs
DTT
DTT + ISRIB
puromycilated NSPs
C
Puromycilated NSPs intensity of IF (normalized to control)
1.5
1.0
0.5
0.0
ns
****
****
**
Control
ISRIB
DTT
DTT + ISRIB

Figure S1. Analysis of the DTT- and Sema3A-induced phosphorylation of eIF2α and its role in axonal translational control – Related to Figure 1 (A) Axons were treated with Sema3A for a timecourse stimulation (5 min, 10 min, 20 min), stained for p-eIF2α, and IF was measured (one-way ANOVA with Bonferroni's Multiple Comparison test). **(B-C)** Axons were incubated with puromycin and co-treated with DTT and ISRIB for 15 min, stained for puromycin, and IF was measured (one-way ANOVA with Bonferroni's Multiple Comparison test). For presentation clarity, brightness/contrast settings were adjusted equally across images collected in the same experiment. Error bars s.e.m. Scale bar 5 μm.

Figure S2

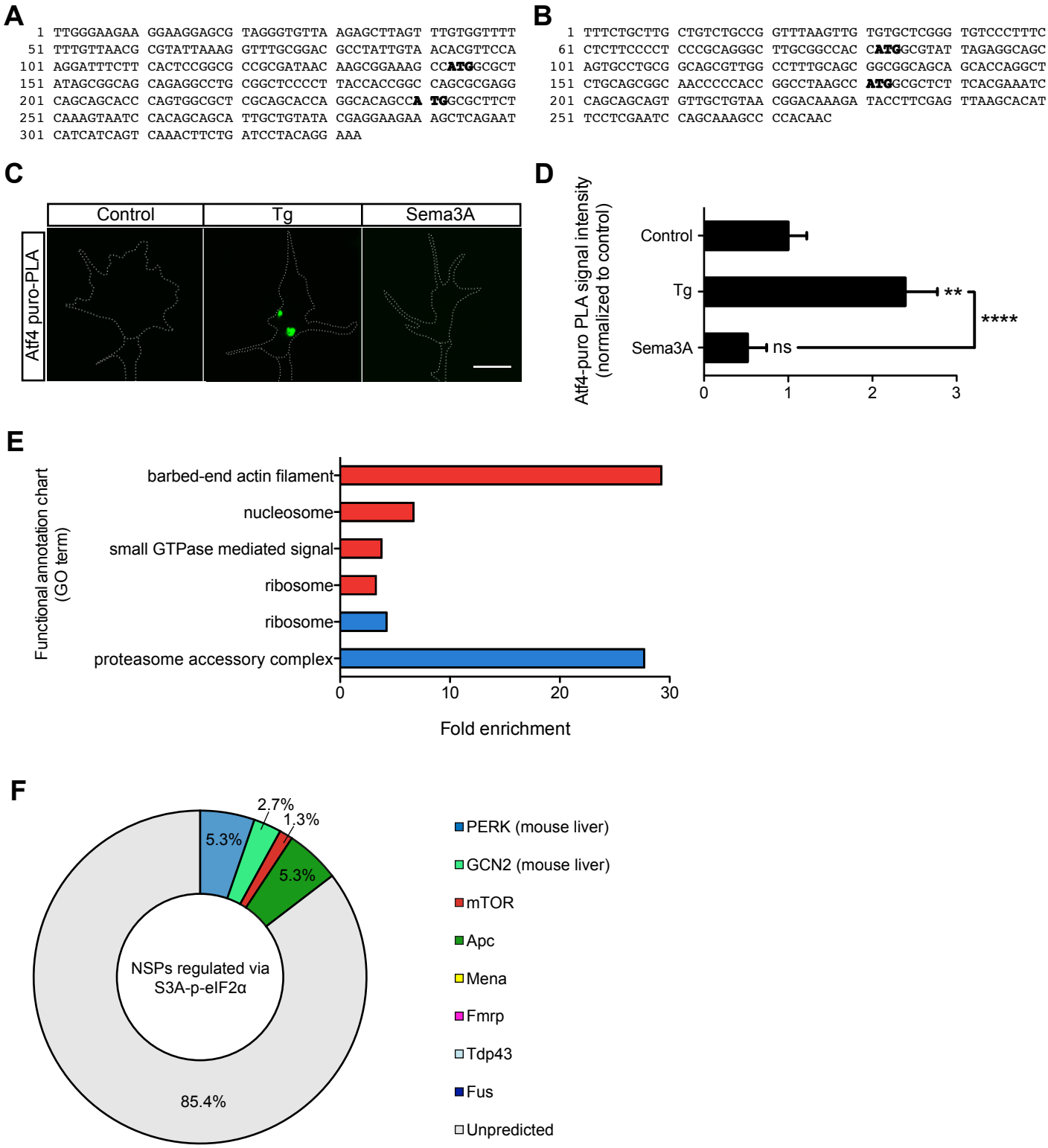
A
1 TTGGGAAGAA GGAAGGAGCG TAGGGTGTTA AGAGCTTAGT TTGTGGTTTT
51 TTTGTTAACG CGTATTAAAG GTTTGCGGAC GCCTATTGTA ACACGTTCCA
101 AGGATTTCTT CACTCCGGCG CCGCGATAAC AAGCGGAAAG CCATGGCGCT
151 ATAGCGGCAG CAGAGGCCTG CGGCTCCCCT TACCACCGGC CAGCGCGAGG
201 CAGCAGCACC CAGTGGCGCT CGCAGCACCA GGCACAGCCA TGGCGCTTCT
251 CAAAGTAATC CACAGCAGCA TTGCTGTATA CGAGGAAGAA AGCTCAGAAT
301 CATCATCAGT CAAACTTCTG ATCCTACAGG AAA
B
1 TTTCTGCTTG CTGTCTGCCG GTTTAAGTTG TGTGCTCGGG TGTCCCTTTC
61 CTCTTCCCCT CCCGCAGGGC TTGCGGCCAC CATGGCGTAT TAGAGGCAGC
101 AGTGCCTGCG GCAGCGTTGG CCTTTGCAGC GGCGGCAGCA GCACCAGGCT
151 CTGCAGCGGC AACCCCCACC GGCCTAAGCC ATGGCGCTCT TCACGAAATC
201 CAGCAGCAGT GTTGCTGTAA CGGACAAAGA TACCTTCGAG TTAAGCACAT
251 TCCTCGAATC CAGCAAAGCC CCACAAC
C
Control
Tg
Sema3A
Atf4 puro-PLA
D
Atf4-puro PLA signal intensity (normalized to control)
Control
Tg
Sema3A
**
****
ns
0
1
2
3
E
Functional annotation chart (GO term)
barbed-end actin filament
nucleosome
small GTPase mediated signal
ribosome
ribosome
proteasome accessory complex
0
10
20
30
Fold enrichment
F
2.7%
1.3%
5.3%
5.3%
NSPs regulated via S3A-p-eIF2α
85.4%
PERK (mouse liver)
GCN2 (mouse liver)
mTOR
Apc
Mena
Fmrp
Tdp43
Fus
Unpredicted

Figure S2. Sema3A-p-eIF2α signaling specifically remodels the nascent axonal proteome – Related to Figure 2 (A) The 5' UTR of Atf4 in *Xenopus laevis* conserves the two uORFs (indicated in bold) previously detected in mouse (Vattem and Wek, 2004). **(B)** The 5'UTR of Atf4 in mouse retinal axons (Shigeoka et al., 2016) exhibits the two uORFs previously detected in Mouse Embryo Fibroblast cells (Vattem and Wek, 2004). **(C-D)** Axons were treated with Tg or Sema3A for 1 h and incubated with puromycin over the last 10 min of the stimulation. PLA was carried out against puromycin and Atf4, and IF was measured (one-way ANOVA with Dunn's Multiple Comparison test). **(E)** Enriched Gene Ontology (GO) terms in the biological process, molecular function and cellular composition categories for the NSPs upregulated (indicated in red) and downregulated (indicated in blue) (p-value < 0.1). **(F)** Percentages of the Sema3A-p-eIF2α-induced NSP changes predicted to be targets of the *trans*-acting elements investigated (Thoreen et al., 2012; Preitner et al, 2014; Vidaki et al., 2017; Darnell et al, 2011; Colombrita et al., 2012; Dang do et al., 2009). For presentation clarity, brightness/contrast settings were adjusted equally across images collected in the same experiment. Error bars s.e.m. Scale bar 5 μm.

Figure S3

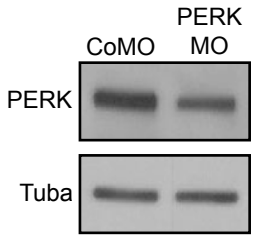

Figure S3. Validation of PERK MO – Related to Figure 3 Immunoblot of eye and brain lysates was probed for PERK in Control and PERK morphants.

Figure S4

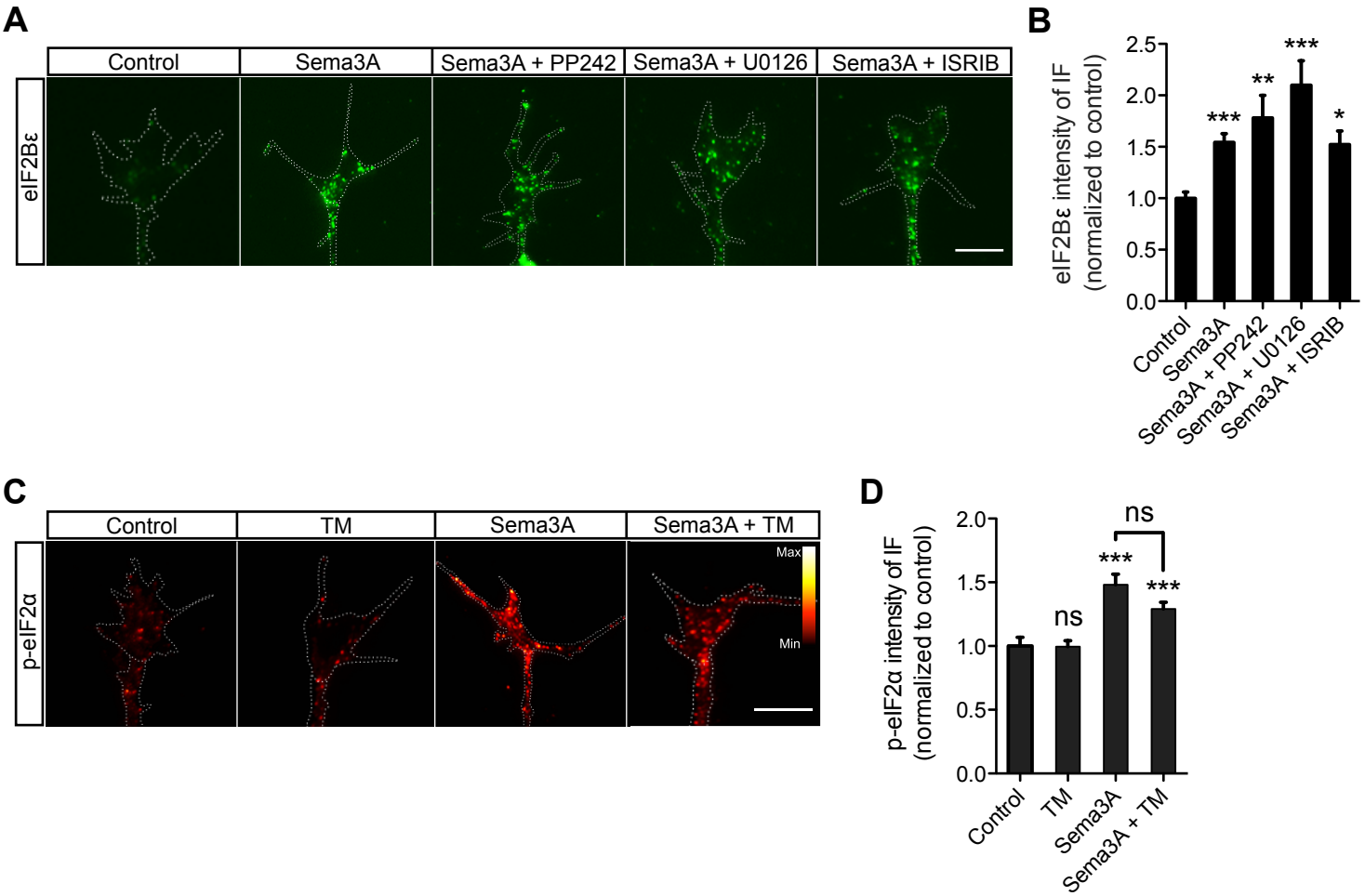
A
Control
Sema3A
Sema3A + PP242
Sema3A + U0126
Sema3A + ISRIB
eIF2Bε
B
eIF2Bε intensity of IF
(normalized to control)
2.5
2.0
1.5
1.0
0.5
0.0
***
**
***
*
Control
Sema3A
Sema3A + PP242
Sema3A + U0126
Sema3A + ISRIB
C
Control
TM
Sema3A
Sema3A + TM
p-eIF2α
Max
Min
D
p-eIF2α intensity of IF
(normalized to control)
2.0
1.5
1.0
0.5
0.0
ns
***
ns
***
Control
TM
Sema3A
Sema3A + TM

Figure S4. Investigation of Sema3A-eIF2Bε-p-eIF2α signaling – Related to Figure 4
(A-B) Axons were co-treated with Sema3A and PP242, U0126 or ISRIB for 5 min, immunostained for eIF2Bε, and IF was measured (one-way ANOVA with Dunn's Multiple Comparison test). **(C-D)** Axons were co-treated with Sema3A and TM for 10 min, stained for p-eIF2α, and IF was measured (one-way ANOVA with Dunn's Multiple Comparison test). For presentation clarity, brightness/contrast settings were adjusted equally across images collected in the same experiment. Error bars s.e.m. Scale bars 5 μm.

Figure S5

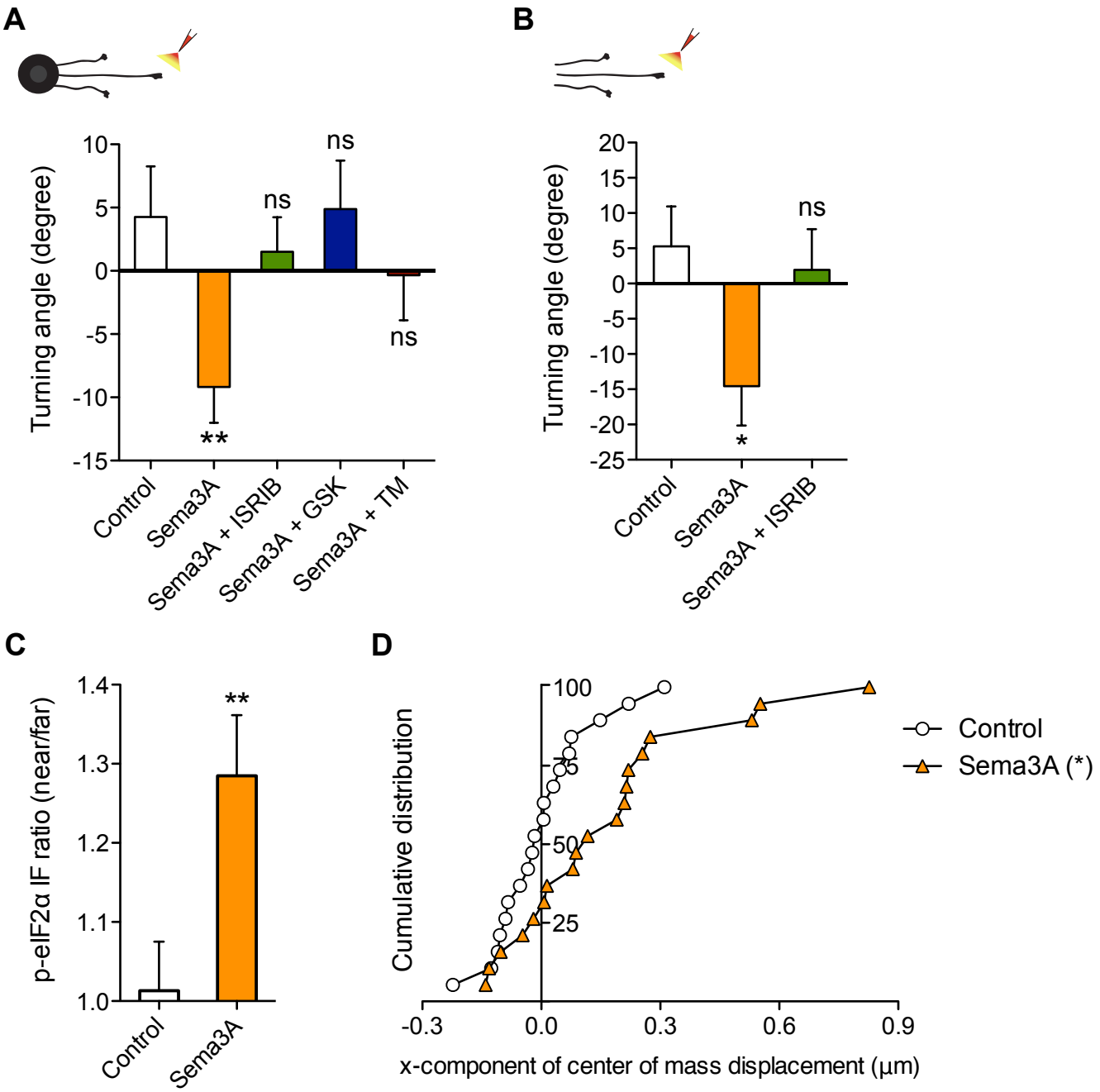
A
B
Turning angle (degree)
10
5
0
-5
-10
-15
ns
ns
ns
**
Control
Sema3A
Sema3A + ISRIB
Sema3A + GSK
Sema3A + TM
20
15
10
5
0
-5
-10
-15
-20
-25
ns
*
Control
Sema3A
Sema3A + ISRIB
C
D
p-eIF2α IF ratio (near/far)
1.4
1.3
1.2
1.1
1.0
**
Control
Sema3A
Cumulative distribution
100
75
50
25
-0.3
0.0
0.3
0.6
0.9
x-component of center of mass displacement (µm)
Control
Sema3A (*)

Figure S5. Spatially polarized phosphorylation of eIF2α mediates Sema3A-induced repulsive turning – Related to Figure 5 (A) Turning assay - a polarized gradient of Sema3A was generated and ISRIB, GSK or TM were bath-applied. Positive values indicate attraction, negative values indicate repulsion (Unpaired t-test). **(B)** Turning assay with somaless axons - a polarized gradient of Sema3A was generated and ISRIB was bath-applied. Positive values indicate attraction, negative values indicate repulsion (Unpaired t-test). **(C)** Asymmetric increase of p-eIF2α assessed by near/far ratio method (Unpaired t-test). **(D)** Cumulative distribution assessing asymmetric increase of p-eIF2α by center of mass method (Unpaired t-test)**.** Error bars s.e.m.

Figure S6

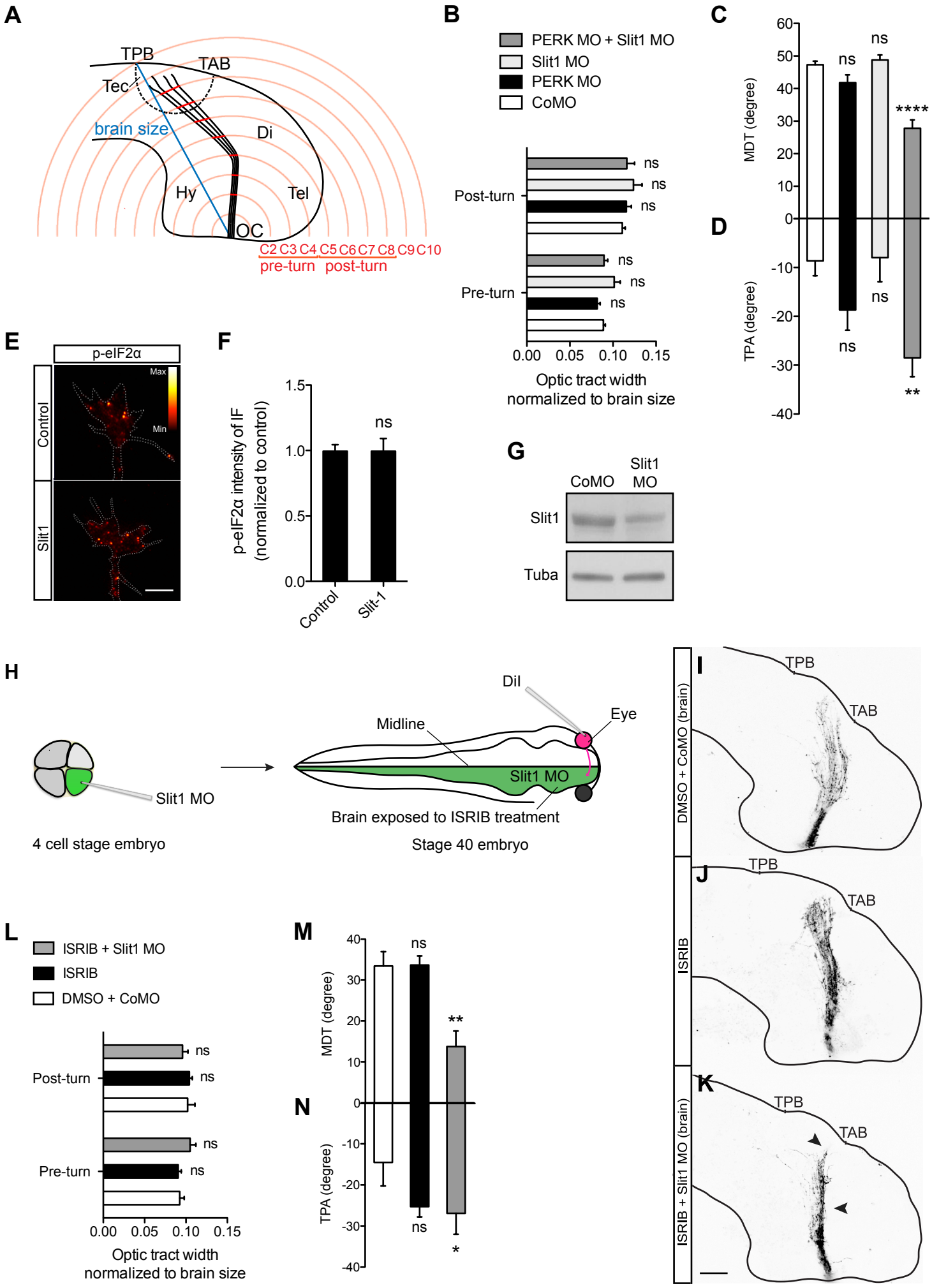
A
TPB
TAB
Tec
brain size
Di
Hy
Tel
OC
C2 C3 C4 C5 C6 C7 C8 C9 C10
pre-turn post-turn
B
PERK MO + Slit1 MO
Slit1 MO
PERK MO
CoMO
Post-turn
Pre-turn
ns
0.00 0.05 0.10 0.15
Optic tract width
normalized to brain size
C
MDT (degree)
60 50 40 30 20 10 0 -10 -20 -30 -40
ns
****
D
TPA (degree)
**
E
p-eIF2α
Control
Slit1
Max
Min
F
p-eIF2α intensity of IF
(normalized to control)
1.5 1.0 0.5 0.0
ns
Control
Slit-1
G
CoMO
Slit1 MO
Slit1
Tuba
H
Slit1 MO
4 cell stage embryo
DiI
Eye
Midline
Slit1 MO
Brain exposed to ISRIB treatment
Stage 40 embryo
I
DMSO + CoMO (brain)
TPB
TAB
J
ISRIB
K
ISRIB + Slit1 MO (brain)
L
ISRIB + Slit1 MO
ISRIB
DMSO + CoMO
Post-turn
Pre-turn
0.00 0.05 0.10 0.15
Optic tract width
normalized to brain size
M
MDT (degree)
40 30 20 10 0 -10 -20 -30 -40
**
N
TPA (degree)
*

Figure S6. PERK-p-eIF2α signaling aids retinotectal axon navigation *in vivo* – Related to Figure 6 (A) Schematic illustrating the quantification of the width of the optic tract. Ten equally spaced concentric circles (C1-C10) were overlaid on the tract images with the center of the circles overlying the optic chiasm (OC) and C10 overlaying the Tectal Posterior Boundary (TPB). The widths of C2-4 and C5-8, corresponding respectively to pre- and post-caudal turn, were averaged. Lastly, the pre- and post-turn widths were normalized to the brain size, defined by the distance between OC and TPB. TAB, Tectal Anterior Boundary; Tec, tectum; Di, Diencephalon; Hy, Hypothalamus; Tel, Telencephalon. **(B)** Quantification of the pre- and post-turn width (two-way ANOVA). **(C)** MDT angle measurements (one-way ANOVA with Bonferroni's Multiple Comparison test). **(D)** TPA measurements - negative values indicate angles pointing towards the TAB (one-way ANOVA with Bonferroni's Multiple Comparison test). **(E-F)** Axons were treated with Slit1 for 10 min, stained for p-eIF2α, and IF was measured (Unpaired t-test). **(G)** Immunoblot of eye and brain lysates was probed for Slit1 in Control and Slit1 morphants. **(H)** Experimental outline to investigate the contribution of p-eIF2α and Slit1 to the axon navigation. Unilateral Slit1 MO injection leaded to a targeted KD in half of the CNS, which was subsequently exposed to ISRIB treatment. **(I-K)** DiI-filled stage 40 retinotectal projections. **(L)** Quantification of the pre- and post-turn width (two-way ANOVA). **(M)** MDT angle measurements (one-way ANOVA with Dunn's Multiple Comparison test). **(N)** TPA measurements – positive values indicate angles pointing towards the TPB, negative values indicate angles pointing towards the TAB (one-way ANOVA with Dunn's Multiple Comparison test). For presentation clarity, brightness/contrast settings were adjusted equally across images collected in the same experiment. Error bars s.e.m. Scale bars 5 μm (E) and 100 μm (I-K).

Table S1. Axonal nascent proteins regulated by Sema3A-p-eIF2α signaling – Related to Figure 2

Table S2

Neurological Disease	NSPs regulated by Sema3A-p-eIF2α signaling
Amyotrophic lateral sclerosis	Sod1, Vcp, Hnrnpa1
Hereditary spastic paraplegia	L1cam, Hspd1
Charcot-Marie-Tooth disease	Vcp
Hypomyelinating leukodystrophy	Hspd1
Syndromic X-linked mental retardation	L1cam
Frontotemporal lobar degeneration	Vcp
Cerebral dysgenesis, neuropathy, ichthyosis, and palmoplantar keratoderma syndrome	Snap29
Early infantile epileptic encephalopathy	Mdh2
ATP synthase deficiency	Atp5a1
Congenital hydrocephalus	L1cam
Hereditary sensory and autonomic neuropathy	Cct5
Familial amyloidosis	Gsn
L1 syndrome	L1cam
Juvenile-onset dystonia	Actb

Table S2. Axonal NSP changes induced by Sema3A-p-eIF2α signaling associated with neurological disorders – Related to Figure 2 Neurological disorders were selected from the *KEGG disease* output.

Graphical Abstract

Table S1

Click here to access/download

Supplemental Videos and Spreadsheets

Table S1.xlsx